NAVAL POSTGRADUATE SCHOOL
Monterey, California

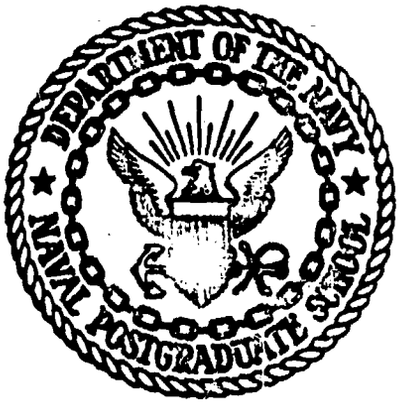

THESIS

A Study of the Crack Damage in Fuel-Filled Tank Walls Due to Ballistic Penetrators

by

Steven Lock Fahrenkrog

March 1976

Thesis Advisor: R. E. Ball

SECURITY CLASSIFICATION OF THIS PAGE (When Data Entered)

REPORT DOCUMENTATION PAGE

READ INSTRUCTIONS BEFORE COMPLETING FORM

1. REPORT NUMBER

2. GOVT ACCESSION NO.

3. RECIPIENT'S CATALOG NUMBER (9)

4. TITLE (and Subtitle) (6)
A Study of the Crack Damage in Fuel-Filled Tank Walls Due to Ballistic Penetrators.

5. TYPE OF REPORT & PERIOD COVERED
Master's Thesis, March 1976

6. PERFORMING ORG. REPORT NUMBER

7. AUTHOR(s) (10)
Steven Lock/Fahrenkrog

8. CONTRACT OR GRANT NUMBER(s)

9. PERFORMING ORGANIZATION NAME AND ADDRESS
Naval Postgraduate School
Monterey, California 93940

10. PROGRAM ELEMENT, PROJECT, TASK AREA & WORK UNIT NUMBERS

11. CONTROLLING OFFICE NAME AND ADDRESS
Naval Postgraduate School
Monterey, California 93940 (11)

12. REPORT DATE
Mar[illegible]76

13. NUMBER OF PAGES
92 pages

14. MONITORING AGENCY NAME & ADDRESS(if different from Controlling Office)
Naval Postgraduate School
Monterey, California 93940
(12) 92p.

15. SECURITY CLASS. (of this report)
Unclassified

15a. DECLASSIFICATION/DOWNGRADING SCHEDULE

16. DISTRIBUTION STATEMENT (of this Report)

** Approved for public release; distribution unlimited.

17. DISTRIBUTION STATEMENT (of the abstract entered in Block 20, if different from Report)

18. SUPPLEMENTARY NOTES

19. KEY WORDS (Continue on reverse side if necessary and identify by block number)

20. ABSTRACT (Continue on reverse side if necessary and identify by block number)

A major goal of the hydraulic ram survivability program for aircraft fuel tanks is the development of analytical-numerical tools for the accurate prediction of damage to the tank due to a ballistic projectile. This report presents a method for predicting the amount of cracking of a penetrated tank wall due to the penetrating projectile and the hydraulic ram loading. The method uses computer codes to predict the

DD FORM 1 JAN 73 1473 (Page 1)
EDITION OF 1 NOV 65 IS OBSOLETE
S/N 0102-014-6601

SECURITY CLASSIFICATION OF THIS PAGE (When Data Entered)

251 450

fluid pressure on the wall and the stresses in the wall. The stresses are compared with empirical data on the fracture of thin cracked plates to obtain a prediction of the final crack length. A comparison of predicted cracks with actual cracks that occurred in plates tested by Naval Weapons Center, China Lake, California is included. Good correlation is obtained when the magnitude of the predicted strains is adjusted to agree with the magnitude of the measured strains by a correction factor.

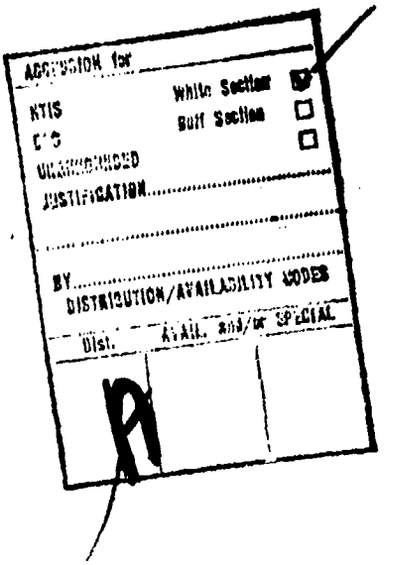

A Study of the Crack Damage in Fuel-Filled Tank Walls Due to Ballistic Penetrators

by

Steven Lock Fahrenkrog
Lieutenant, United States Navy
B.A., Moorhead State College, 1969

Submitted in partial fulfillment of the requirements for the degree of

MASTER OF SCIENCE IN AERONAUTICAL ENGINEERING

from the

NAVAL POSTGRADUATE SCHOOL
March 1976

Author Steven L. Fahrenkrog

Approved by: M. A. Gallo
Thesis Advisor

R. E. Lindem
Second Reader

C. W. Bell
Chairman, Department of Aeronautics

J. R. Stanley
Academic Dean

ABSTRACT

A major goal of the hydraulic ram survivability program for aircraft fuel tanks is the development of analytical-numerical tools for the accurate prediction of damage to the tank due to a ballistic projectile. This report presents a method for predicting the amount of cracking of a penetrated tank wall due to the penetrating projectile and the hydraulic ram loading. The method uses computer codes to predict the fluid pressure on the wall and the stresses in the wall. The stresses are compared with empirical data on the fracture of thin cracked plates to obtain a prediction of the final crack length. A comparison of predicted cracks with actual cracks that occurred in plates tested by Naval Weapons Center, China Lake, California is included. Good correlation is obtained when the magnitude of the predicted strains is adjusted to agree with the magnitude of the measured strains by a correction factor.

TABLE OF CONTENTS

LIST OF TABLES

LIST OF FIGURES

ACKNOWLEDGEMENT

The author would like to thank the following people for their help in making this study.

Special thanks to Mr. W. K. Fung of Naval Weapons Center, China Lake, California, for his support and timely forwarding of pictures, motion pictures, and test plates from the NWC tests 5-HR, 6-HR, and 7-HR.

Thanks to Assistant Professors A. J. Perkins and G. R. Edwards and Technician R. F. Edwards of the Department of Mechanical Engineering for their help and instruction concerning the use of the Naval Postgraduate School's Scanning Electron Microscope.

Thanks to Associate Professor G. H. Lindsey of the Department of Aeronautics for his guidance concerning the research on fracture and his constructive criticism as second reader.

Finally special thanks to Associate Professor R. E. Ball of the Department of Aeronautics for his help as Thesis Advisor, without which this study would not have been possible.

I. INTRODUCTION

A. FUEL TANK DAMAGE

Studies of aircraft battle damage reports from the Viet Nam War have pointed out the vulnerability of sophisticated aircraft to small arms ground fire and to surface-to-air missiles. Since aircraft fuel cells have the largest surface area and volume of all the vulnerable aircraft components, and in light of increased aircraft costs and continued decreases in the national defense budget, aircraft fuel cell survivability analysis and design are absolutely necessary.

Since projectiles represent one of the greatest threats to aircraft fuel tanks, projectile-fuel tank interaction is of particular interest. A projectile that penetrates a fluid-containing cell causes damage many times greater than a projectile penetrating an empty cell. This interaction of a projectile with a fluid-containing cell is called the hydraulic ram phenomenon.

The hydraulic ram phenomenon can be divided into five phases which are named after the dominant mechanism of projectile energy dissipation. The phases are:

1. "Penetration phase" ... projectile energy is lost in "punching" a hole in the entry wall.
2. "Shock phase" ... projectile protrusion into the fluid drives a hemispherical shock wave into the tank liquid.

3. "Drag phase" ... projectile energy is dissipated by form drag as it passes through the fluid, and a cylindrical air- and vapor-filled cavity is formed.
4. "Exit phase" ... projectile punches a hole in the exit wall if first three phases have not dissipated all of the projectile energy.
5. "Cavity oscillation phase" ... results from the growth and eventual collapse of the drag phase cavity.

The interrelationships of these phases are shown in Fig. 1, and more detailed explanations of each phase may be found in Refs. 1, 2, 3 and 4. It should be noted that there is no precise beginning or end of any particular phase.

The complete penetration of a fluid-containing cell by a ballistic projectile can have a catastrophic effect on the cell exit wall, as can be seen in Figs. 2 and 3. However, when the projectile velocity is lowered slightly comparatively small damage may occur as can be seen in Figs. 4 and 5. Although the shock phase and the cavity oscillation phase can affect the exit wall response, the drag phase and the exit phase are usually the most important when considering damage to exit walls. During these two phases, the exit wall is loaded by pressures due to both the penetrating projectile itself and the fluid motion toward the wall caused by the earlier shock and drag phases. These pressures cause the relatively large and small damage shown in Figs. 2-5. The ability to predict

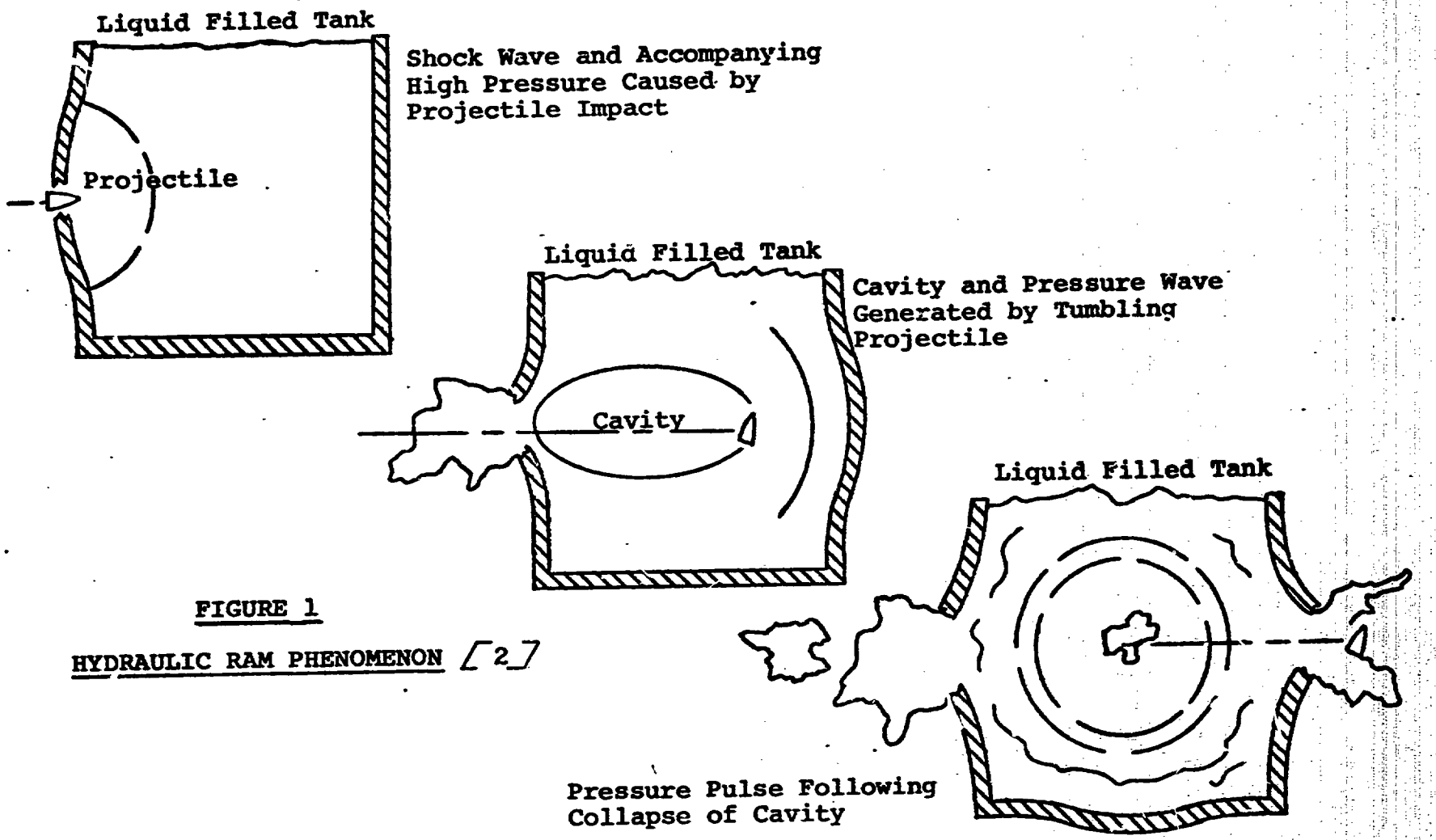

FIGURE 1

HYDRAULIC RAM PHENOMENON [2]

FIGURE 2. NWC 6-HR-3 Series Test Plate
Thickness 0.063 inch
Projectile velocity 2358 fps

FIGURE 3. NWC 6-HR-14 Series Test Plate
Thickness 0.063 inch
Projectile velocity 2212 fps

FIGURE 4. NWC 6-HR-8 Series Test Plate
Thickness 0.063 inch
Projectile velocity 2118 fps

FIGURE 5. NWC 6-HR-15 Series Test Plate
Thickness 0.063 inch
Projectile velocity 2127 fps

the amount of damage to the exit wall is important in fuel cell survivability analysis and design because:

1. a prediction of the time required for the fuel in a tank to empty can be made.
2. designers can predict the amount of fuel dumped into an engine inlet from an integral fuselage-intake fuel tank.
3. designers can estimate the amount of fuel atomization that occurs and the associated fire hazard.

B. PREVIOUS HYDRAULIC RAM AND STRUCTURAL RESPONSE STUDIES

Due to the increased emphasis that has recently been placed on aircraft survivability, a large amount of research effort has been devoted to the development of an understanding of the hydraulic ram effect and the associated fluid-structure interaction. The Hydraulic Ram Project conducted at the Naval Weapons Center (NWC), China Lake, California, is of particular interest here. Phase One of that project resulted in a digital computer code, Ref. 5, developed by Lundstrom and Fung that predicts the drag phase fluid pressure throughout a rectangular tank due to ballistic penetrators. The code was based upon an analytical model, Ref. 2, and the empirical data of Ref. 6, which was also obtained during Phase One.

Phase Two of the NWC Hydraulic Ram Project was concerned with the description of the fluid-structure interaction during the loading of the fuel tank exit wall due to the hydraulic ram pressure. In support of this goal, detailed measurements

of the strains at several locations on the tank exit wall were obtained from an extensive series of 12.7 mm API ballistic penetration tests on rectangular, fluid-filled tanks. A detailed description of the test set-up and the results are given in Ref. 7.

An analytical and experimental hydraulic ram program has been conducted at the Naval Postgraduate School (NPS) in conjunction with the NWC program for approximately three years. As part of this program a ballistic range, consisting of a 22 caliber rifle and a fluid-containing cubic tank, was built and used to obtain fluid pressure and entry wall strain measurements for various projectile sizes and energy levels. The results of the various experiments conducted are given in Refs. 8-18.

The goal of the analytical phase of the NPS program has been to develop methods of analysis that will accurately predict the structural response of the tank walls to loadings caused by hydraulic ram. The results of this effort are given in Refs. 11 and 18-22. Two structural analysis digital computer codes, BR-1 and SATANS, have been modified by Ball to predict the stresses and strains in the walls of a fluid-containing tank as a function of time. It was necessary to modify the two computer codes in order to account for the fluid-structure interaction and cavitation. One-dimensional piston theory was used to approximate the fluid-structure interaction. Information on the modified codes, BR-1HR for rectangular walls and SATANS for circular walls, and their

use is given in Ref. 23 and 24. Both BR-1HR and SATANS use the NWC Hydraulic Ram Pressure code described in Ref. 5 to determine the pressure applied to the tank wall. A comparison of the exit wall strains predicted by SATANS with the strains measured by NWC is given in Ref. 25.

C. EXIT WALL FRACTURE STUDY

This report presents the results of research directed at understanding and predicting the fracture of fuel tank exit walls caused by the hydraulic ram phenomenon. The information in Section II begins with a description of several common types of fractures. Section II continues with a few of the current theories of fracture that were considered as possible theories for predicting the extent of fracture in the exit walls. In Section III is given a brief description of the hydraulic ram exit wall tests conducted at NWC for three different velocity levels. In Section IV, the fractured plates, strain gauge readings, and high speed motion pictures from the NWC tests are examined in order to determine the fracture process and to guide the development of a fracture prediction method. In Section V, the proposed method of fracture prediction is described, and a comparison of the predicted fracture length to the actual fracture length that occurred in the NWC low velocity tests is presented. Section VI contains the conclusions of this study and recommended areas for further study.

II. FRACTURE AND THEORIES OF FRACTURE

An understanding of fracture and the theories of fracture is important when predicting the damage to the fuel cell exit wall. When stress causes a material to break into two or more parts the material is said to have fractured. Although fracture is a relatively common occurrence, its true nature is still not completely understood. One of the most convenient ways to describe fracture and the theories of fracture centers on the size of the fracture region of interest. There are usually three size levels of concern; atomistic level (dimensions on the order of 10^{-8} in.), microscopic level (dimensions on the order of 5×10^{-4} in.), and macroscopic level (dimensions on the order of 10^{-1} in. or greater). However, as pointed out by Drucker [Ref. 26], the atomistic and microscopic levels are better suited to describing fracture than predicting it. Also, because the accuracy of the predicted stress-strain histories at these two levels is debatable, all three levels will be used to describe fracture, but only the macroscopic theories of fracture will be discussed.

A. TYPES OF FRACTURE

At the atomistic level individual atoms and molecules are the center of attention. At this level, fracture consists of two types; cleavage and shear. Cleavage is defined as the breaking of atomic bonds normal to the fracture plane, and

shear is defined as the process of shearing the bonds across the fracture plane.

At the microscopic and macroscopic levels the discussion becomes more complicated. The microscopic level centers on the individual crystals of material, and the macroscopic level centers on the total specimen. In both cases there are three classes of fracture; cleavage, shear, and grain boundary. The first two can be described as transcrystalline and the third can be described as intercrystalline. Grain boundary or intercrystalline fracture usually occurs under a static loading condition that leads to creep fracture and failure due to stress corrosion. Because this loading condition and these types of failure are not found in the hydraulic ram process, intercrystalline fracture will not be considered further.

Microstructurally, cleavage fracture can be distinguished from shear fracture by a consideration of the characteristic lattice plane on which the fracture occurs. To illustrate which plane is associated with the two types of fracture, consider the unit cell of a body centered cubic crystal such as found in iron or steel, shown in Fig. 6. The cleavage plane $\langle 100 \rangle$ of Fig. 6(a) locates the cleavage fracture while it is the slip plane $\langle 110 \rangle$ of Fig. 6(b) on which the shear fracture operates. Table I gives the cleavage and shear planes for various crystalline structures and materials. As can be seen in Table I, aluminum (Al) does not have a cleavage plane.

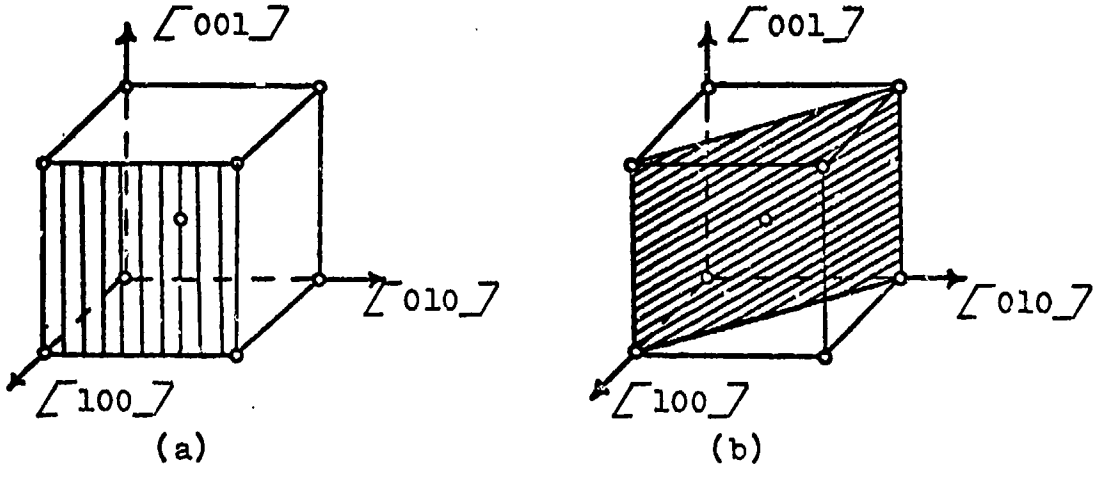

(100) cleavage plane (110) slip plane

FIGURE 6. Characteristic transcrystalline fracture planes in iron or steel [27]

TABLE I

Cleavage and Shear Planes for Various Crystal Structures and Materials [28]

Crystal Structure	Example	Cleavage Plane	Primary Shear Planes
BCC	Li,Na,K,V,Cr, Fe,most steels, Mn,Cb,Mo,W,Ta	[100]	[112],[110]
FCC	Cu,Ag,Au,Al,Ni, brass,300 series stainless steels	None	[111]
HCP	Be, Mg, Zn, Sn, Ti, U, Cd, graphite	[1000]	[1122],[1010], [1000]

Fractography is the macroscopic and/or microscopic examination of the fracture surface and is used to provide information on the micromechanism of fracture. On a macroscopic level the general appearance of the cleavage fracture surface is bright, granular, and crystalline while the shear fracture is dull gray, fibrous, and silky. On the microscopic level the examination of fracture surfaces can be accomplished with either a light microscope or scanning electron microscope (SEM). The interested reader is directed to Ref. 29 for a complete discussion of microfractography and its interpretation.

Figure 7 shows the general appearance of cleavage and shear fractures on the macroscopic and microscopic levels under uniaxial tensile loading. Macroscopically, besides the general appearance already discussed, cleavage fractures appear flat or square as shown in Fig. 7(a). On the other hand, shear fractures appear either slanted or chisel-pointed as shown in Fig. 7(b).

Another common way of distinguishing different fracture types is based on the amount of plastic flow involved in the fracture process. Ductile fracture is characterized as having a considerable amount of plastic flow associated with it. Brittle fracture, in contrast, is characterized as having very little or no plastic flow. Because these two terms are not consistently associated with any single one of the terms already discussed, they greatly confuse the issue. Table II may be helpful in elucidating the terminology, if it is remembered that the two right-hand terms of the third row

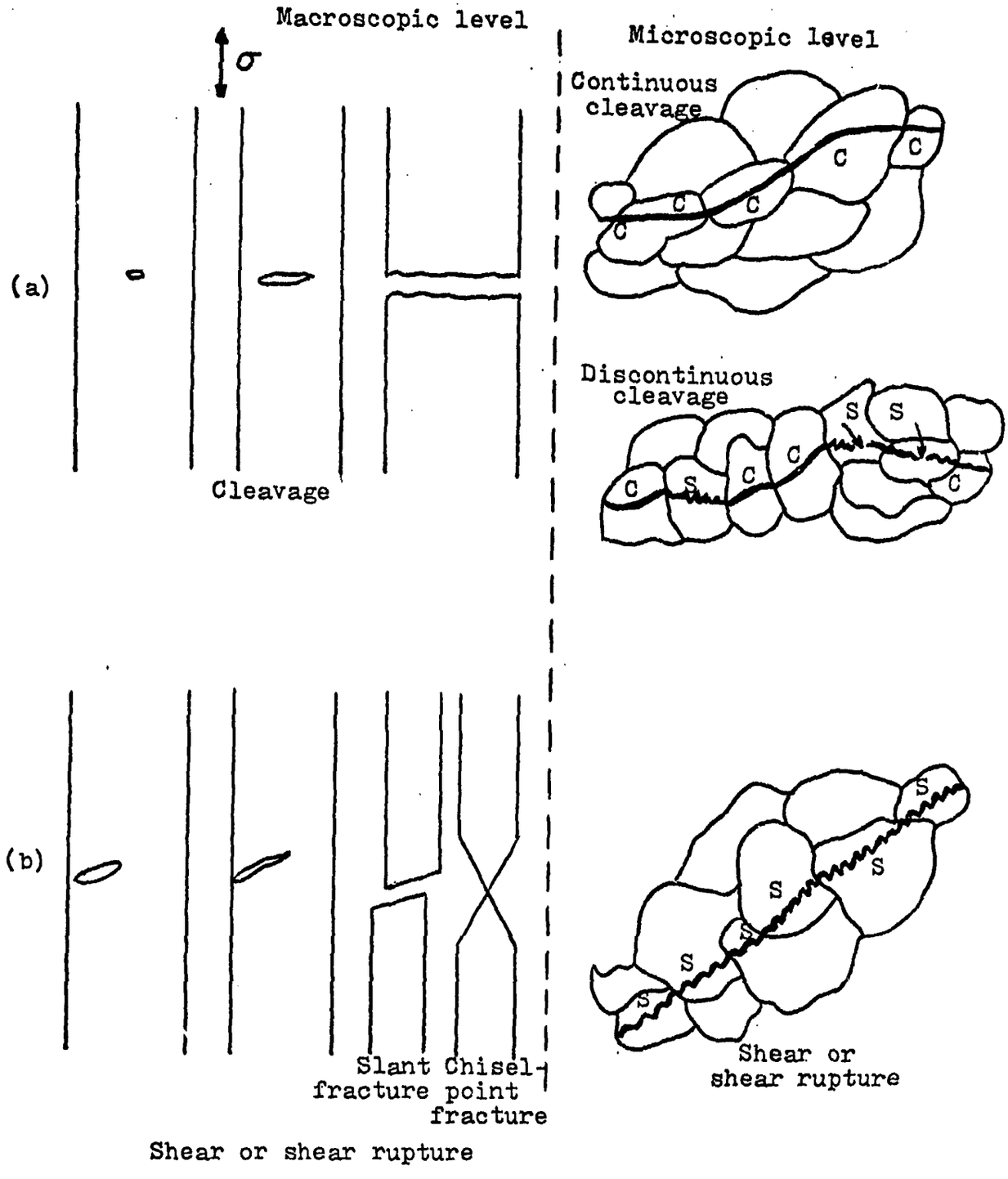

FIGURE 7. Comparison of Cleavage and Shear Fractures at Macroscopic Level and Microscopic Level

TABLE II

Transcrystalline fracture and its terminology [27]

Basis of classification	Types of transcrystalline fracture	
Crystallography	shear	cleavage
Fracture appearance	fibrous	granular
Strain or strain energy at fracture	ductile	brittle

are often used either interchangeably with the term of the first row in the same column or as adjectives describing either term of the first row [27].

Since fuel cell walls are often thin sheets of material, the fracture of sheet material in tension is of interest. Tetelman and McEvily [Ref. 28] and Ryder and Smale [Ref. 29] describe the two macroscopically different types of behavior illustrated in Fig. 8. Both types of behavior are characteristic of shear fracture. Figure 8(A) shows a relatively brittle process that would be expected in thick plates and round tensile bars. Figure 8(B), on the other hand, shows a relatively ductile process which would be expected in thin sheets, particularly those sheets made of the Duralumins.

B. MACROSCOPIC FRACTURE THEORIES

Many theories of fracture have been developed at the macroscopic level. The various theories range from simple to complex in nature. Some assume an unflawed specimen, and others do not. Only a few of the more widely accepted theories will be described.

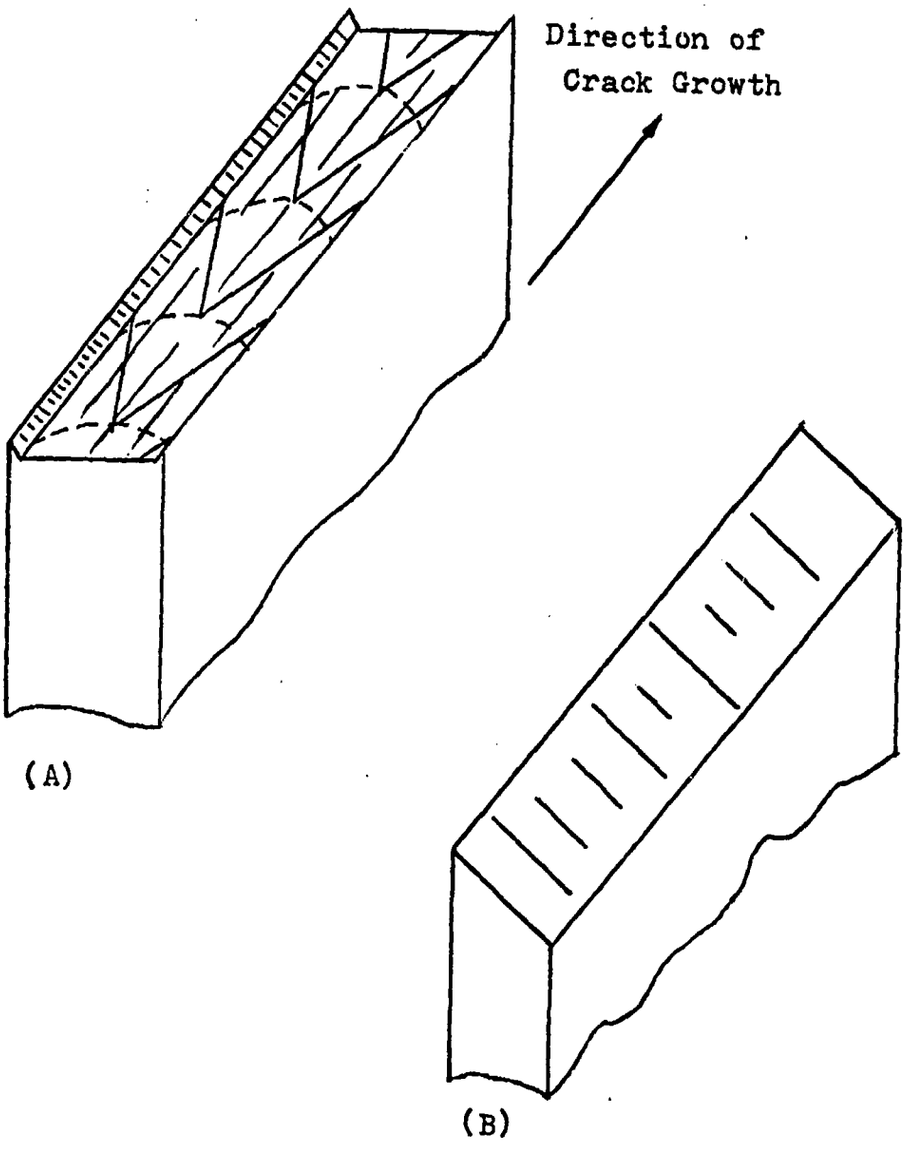

FIGURE 8. Two Modes of Tensile Fracture Observed in Sheet Specimens: (A) Brittle Normal Fracture; (B) Ductile 45° Fracture [30]

The first three theories are similar in that they assume a specimen with no defects and use either the tensile (or compression) ultimate strength, σ_{ut}, or the ultimate shear strength of the material as the criterion for fracture. The simplest of these macroscopic theories is the maximum tensile stress, or Rankine, theory. This theory would predict fracture if the maximum principal stress of a given specimen was greater than or equal to the tensile (or compressive) ultimate strength. The theory is generally considered reasonable only when failure occurs by cleavage fracture.

The maximum shear stress, or Tresca, theory proposes that fracture will occur when the maximum shear stress exceeds the ultimate shear strength of the material. When used to predict the fracture of polycrystalline materials, such as aluminum, this theory usually also requires the definition of a criterion of ductility.

The last theory of this type, closely related to the maximum shear stress theory, is the octahedral shear stress theory. This theory is also known as the maximum distortional energy theory or the von Mises theory. In terms of the principal stresses σ_1, σ_2 and σ_3 this theory may be expressed as

$$(\sigma_2 - \sigma_1)^2 + (\sigma_3 - \sigma_1)^2 + (\sigma_3 - \sigma_2)^2 = 2\sigma_{ut}^2$$

This theory is generally used for materials that exhibit large amounts of plasticity or flow before fracture. The fracture criteria for these three theories in plane stress

are compared in Fig. 9 by plotting them on a graph of biaxial stress σ_1 and σ_2.

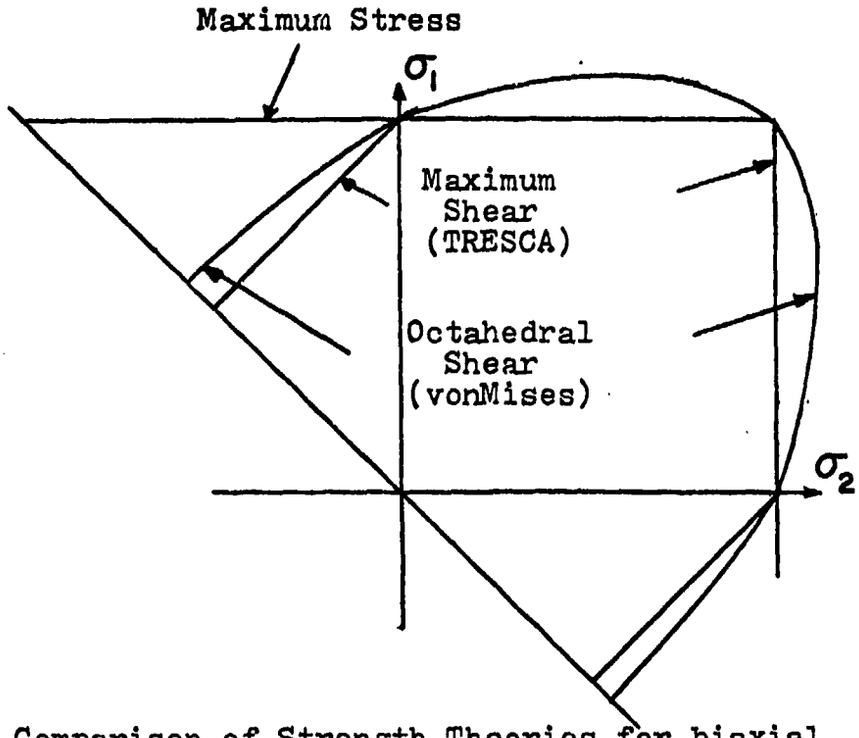

FIGURE 9. Comparison of Strength Theories for biaxial stress

If a defect, such as a crack or hole, exists in the specimen, the fracture analysis must determine whether or not the crack will propagate under a given load. This problem is usually treated using the modifications of the Griffith crack theory proposed by Irwin [Ref. 31] and Orowan [Ref. 32].

These modifications led to a concept of fracture instability based on a stress-intensity factor K at the root of a stationary or slowly growing crack or defect in a body. The elastic confinement of the material governs the degree of plain strain at the tip of the crack. Therefore the critical stress intensity, K_c, is assumed to be a material property. The theory proposes that when the loading produces a stress intensity equal to the critical one, the crack propagates rapidly over the cross section. The critical stress-intensity factor can be related to the strain-energy release rate since, at the instability of crack extension, the energy release rate is equal to the rate of change of strain energy with respect to crack area when the displacements of the externally applied loads are held constant during the incremental crack extension. Both the strain-energy release rate and the stress-intensity factor are functions of loading, structure geometry and size, and crack orientation.

The stress-intensity factor also varies with the relative motion of the crack surfaces, or what is called the modes of fracture. There are three basic modes or combinations of them. Mode I, the opening mode, is characterized by the crack surfaces separating, perpendicular to the maximum tensile stress. Mode II, the shear mode, is characterized by the crack surfaces shearing in a direction perpendicular to the crack front. Mode III, the tearing mode, is characterized by the crack surfaces shearing in a direction parallel to the crack front. For example, the stress-intensity factor

$$K_I = \sigma(\pi a)^{\frac{1}{2}}$$

is for an infinite plate under a uniaxial average tension stress σ with a crack length of 2a perpendicular to the direction of applied stress. The subscript I denotes the opening mode. Fast crack extension occurs when $K_I \geq K_{Ic}$. Thus, the critical stress for fracture σ_c is

$$\sigma_c = K_{Ic}(\pi a)^{-\frac{1}{2}}$$

Note that σ_c varies inversely with the square root of the crack length. Therefore, if the crack is sufficiently long, fracture will occur when the average stress in the plate is below the yield strength.

Modifications to include plasticity around the crack tip make it possible to handle materials that exhibit semi-brittle or ductile fractures. The reader is directed to Ref. 33 for a more complete discussion of this theory and its various modifications.

The fracture criteria discussed in this Section were each considered for use in the crack prediction method described in Section V. Those theories that pertain to unflawed specimens such as the maximum shear stress theory or the octahedral shear stress theory were disregarded because they are generally only considered relevant for unflawed specimens. The modified Griffith crack theory described was not used because the selection of the appropriate modifications to

the theory for the test plate geometry considerations, and the selection of an appropriate plane stress critical stress intensity, K_c, to use, was not considered feasible at the present time. Since the theoretical fracture criteria did not appear useable for the reasons mentioned, a method based on empirical data was formulated. The method is presented in Section V.

III. THE NWC EXIT WALL TEST PROGRAM

A. EXPERIMENTAL SET-UP

During the last three years the Naval Weapons Center (NWC), China Lake, California, has conducted experimental work on the hydraulic ram phenomenon which is directly related to this study. In this section the relevant part of this work will be briefly discussed.

A series of tests was conducted at NWC to measure the strains at four locations on the exit wall of a simulated aircraft fuel tank subjected to hydraulic ram effects. The tests were conducted at NWC, using 12.7 mm API ballistic projectiles fired at a fluid filled, rectangular tank. The tank is 60 inches wide by 60 inches high, with 22 inches between the entry and exit walls, and has an open top. A schema of the tank is shown in Fig. 10. The central portion of the entry wall is a stretched rubber membrane and the central portion of the exit wall is a 20-inch by 20-inch by 0.125-inch test plate of 2024-T3 aluminum clamped to a 0.25-inch steel wall. The exit wall with a damaged test plate is shown in Fig. 11. The edge clamping of the test plates was obtained by compression (friction) between two rubber gaskets around the outer perimeter of the plate. A pin through the plate at two diametrically opposed corners provided additional edge support. A schema of the test set-up is shown in Fig. 12.

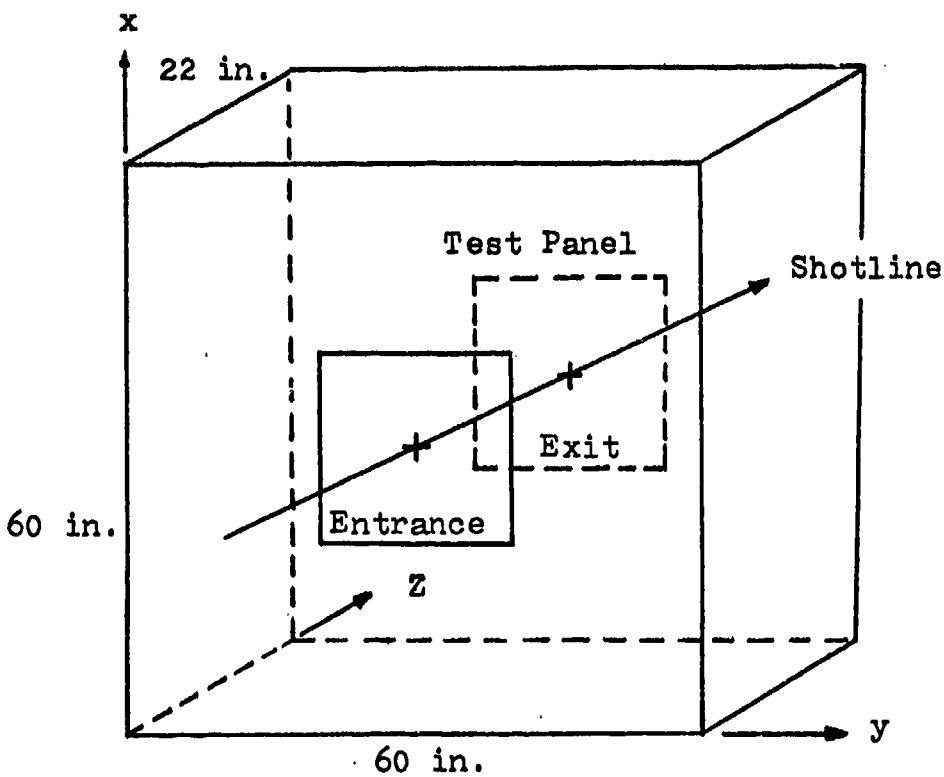

FIGURE 10. Schema of Test Tank

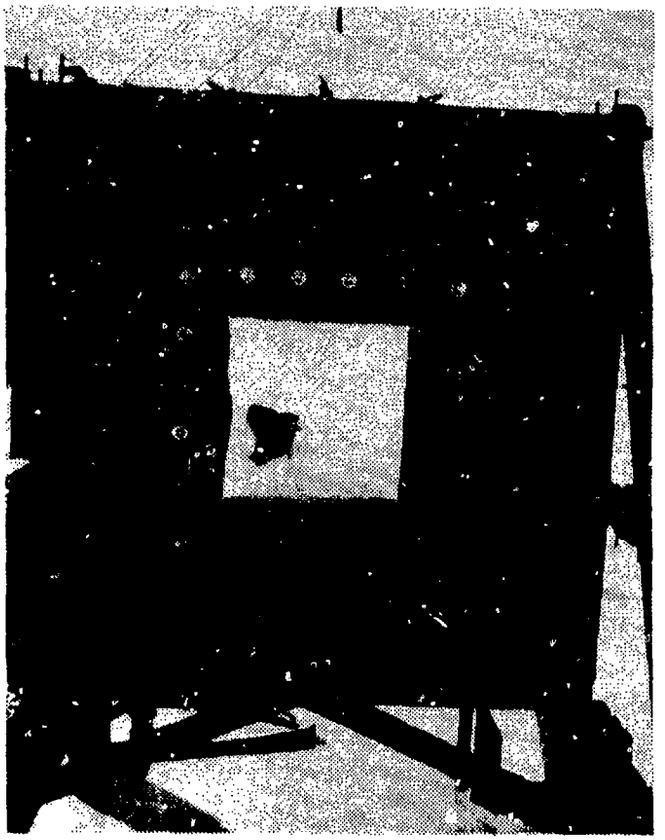

FIGURE 11. Test Plate Mounted in Exit Wall of Test Tank

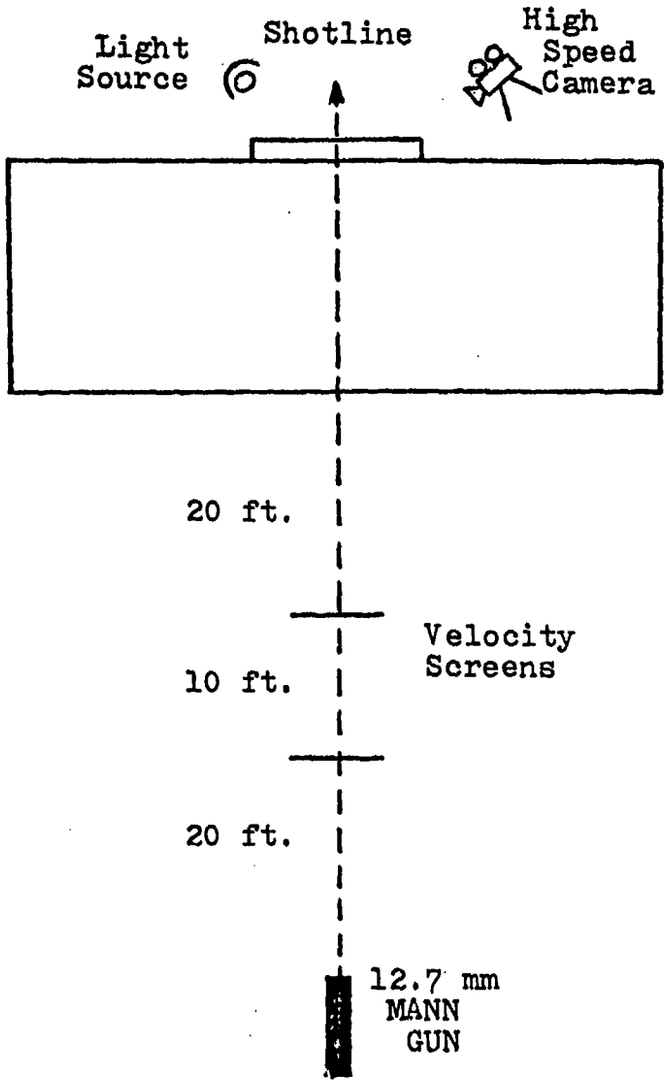

FIGURE 12. Schema of Test Set Up

During this series of tests fourteen 12.7mm API projectiles were fired at the tank with velocities between 1300 fps and 2800 fps. The strains on the wet and dry surfaces of the exit wall were measured at the four locations shown in Fig. 13 for each shot. The strains at each location were measured in the two directions indicated by the short lines in Fig. 13. Pressures were measured at five locations along the projectile trajectory inside the tank. High-speed motion pictures of the exit wall response were taken looking at the dry side of the exit wall.

B. EXIT WALL DAMAGE

Table III lists the projectile velocity and the extent of damage for each shot, and Figs. 14-26 show the damage looking at the dry side of each test plate. In general, the low velocity projectiles caused limited bulging of the exit wall with short cracks approximately three inches in length emanating from the penetration point. The high velocity projectiles, on the other hand, caused severe tearing of the wall with several cracks emanating from the exit hole and running to the edges of the plate. A more detailed description of the experimental set-up and a presentation of all exit wall strain data, is given in Ref. 7. Selected results from the NWC tests will be presented in Section V where a comparison between the experimental results and analytical results is made.

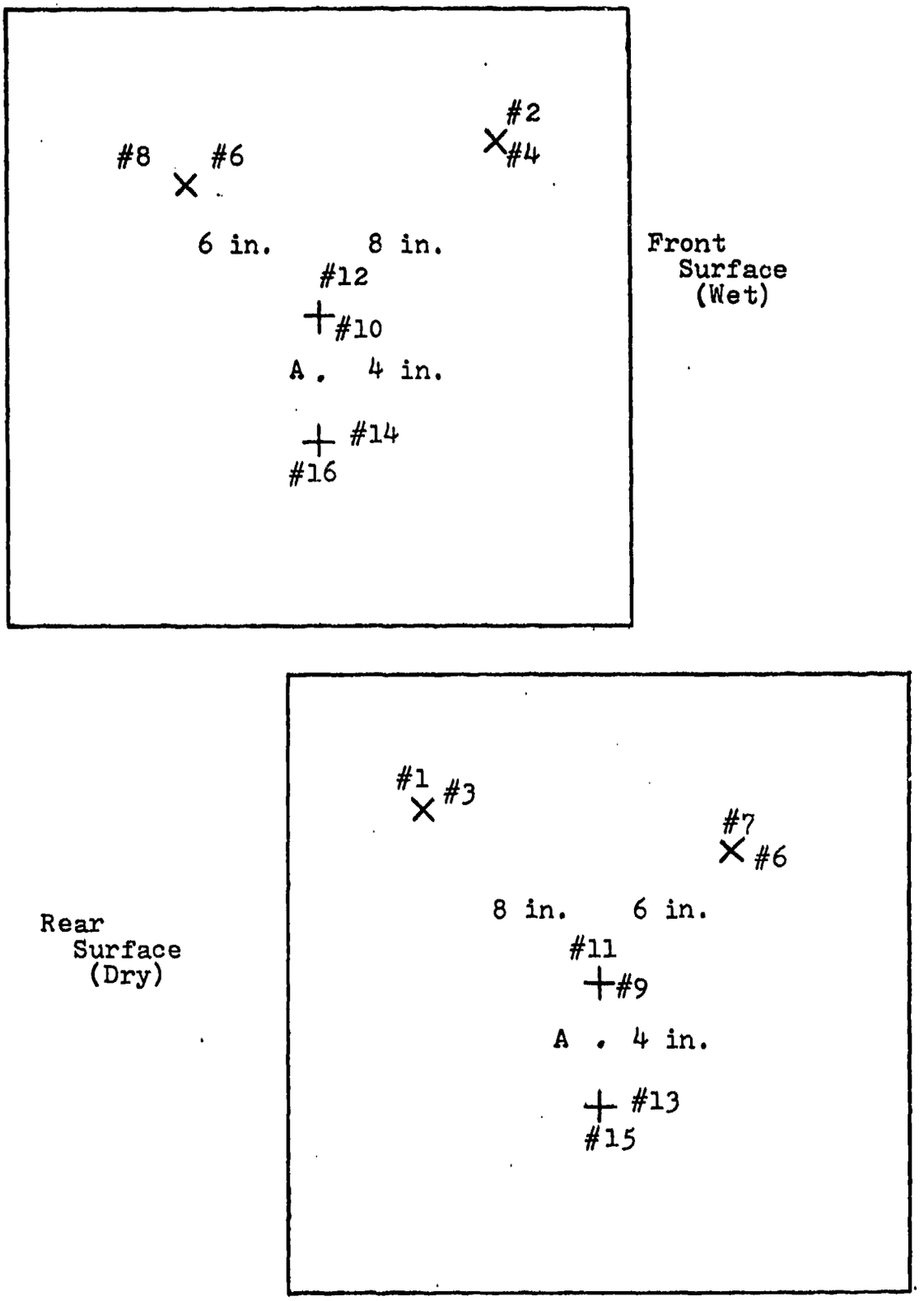

FIGURE 13. Location of Strain Gages and Point "A" for the 7-HR-14 Shot

TABLE III

Projectile Velocity and Extent of Exit Wall Damage

Shot	Velocity (fps)	Damage
1	2,200	Cigar-shaped hole 3 in. long
2	2,217	Small circular hole 1.5 in. in dia. with one 5 in. crack and one 1 in. crack
3	2,254	One 11 in. and one 9 in. cracks
4	2,198	Cigar-shaped hole 3 in. long
5	2,113	Cigar-shaped hole 3 in. long
6	2,763	Circular hole 3 in. in dia. including petaling with one 10 in. crack and one 8 in. crack
7	2,673	5 in. hole with several 5 in. cracks and petaling
8	2,643	5 in. hole and several 5 in. cracks and petaling
9	2,718	Bulged plate with 5 in. cigar-shaped hole and two 1.5 in. cracks
10	1,347	One 3 in. crack and two 1 in. cracks
11	1,386	Cigar-shaped hole 2 in. long and two 2 in. cracks
12	1,366	Cigar-shaped hole 2.5 in. long and four 1.5 in. cracks
13	1,396	Not available
14	1,389	Very small hole with one 3 in., one 2 in., and one 1.5 in. cracks

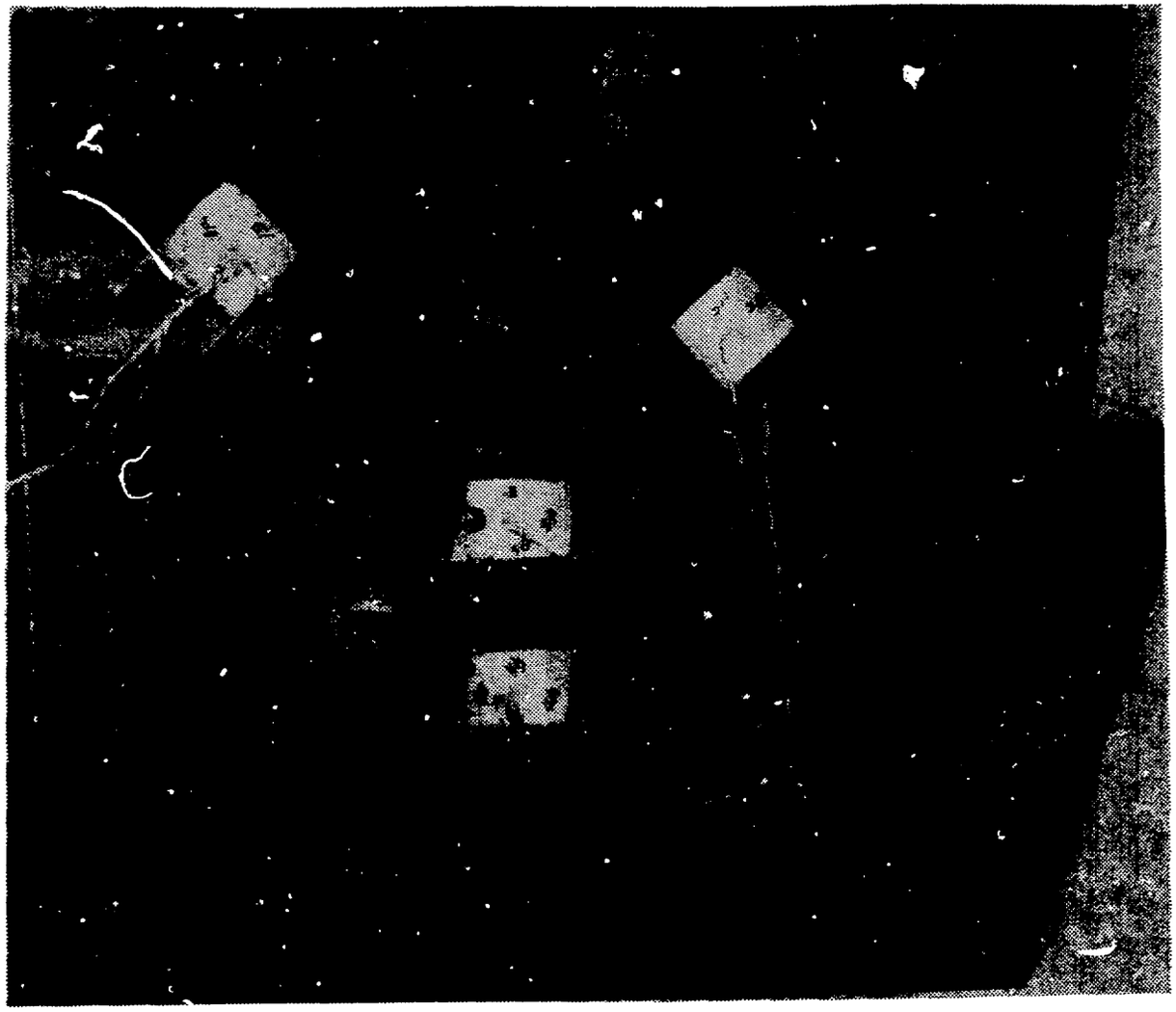

FIGURE 14. 7-HR-1 (Test Plate After Shot)

FIGURE 15. 7-HR-2 (Test Plate After Shot)

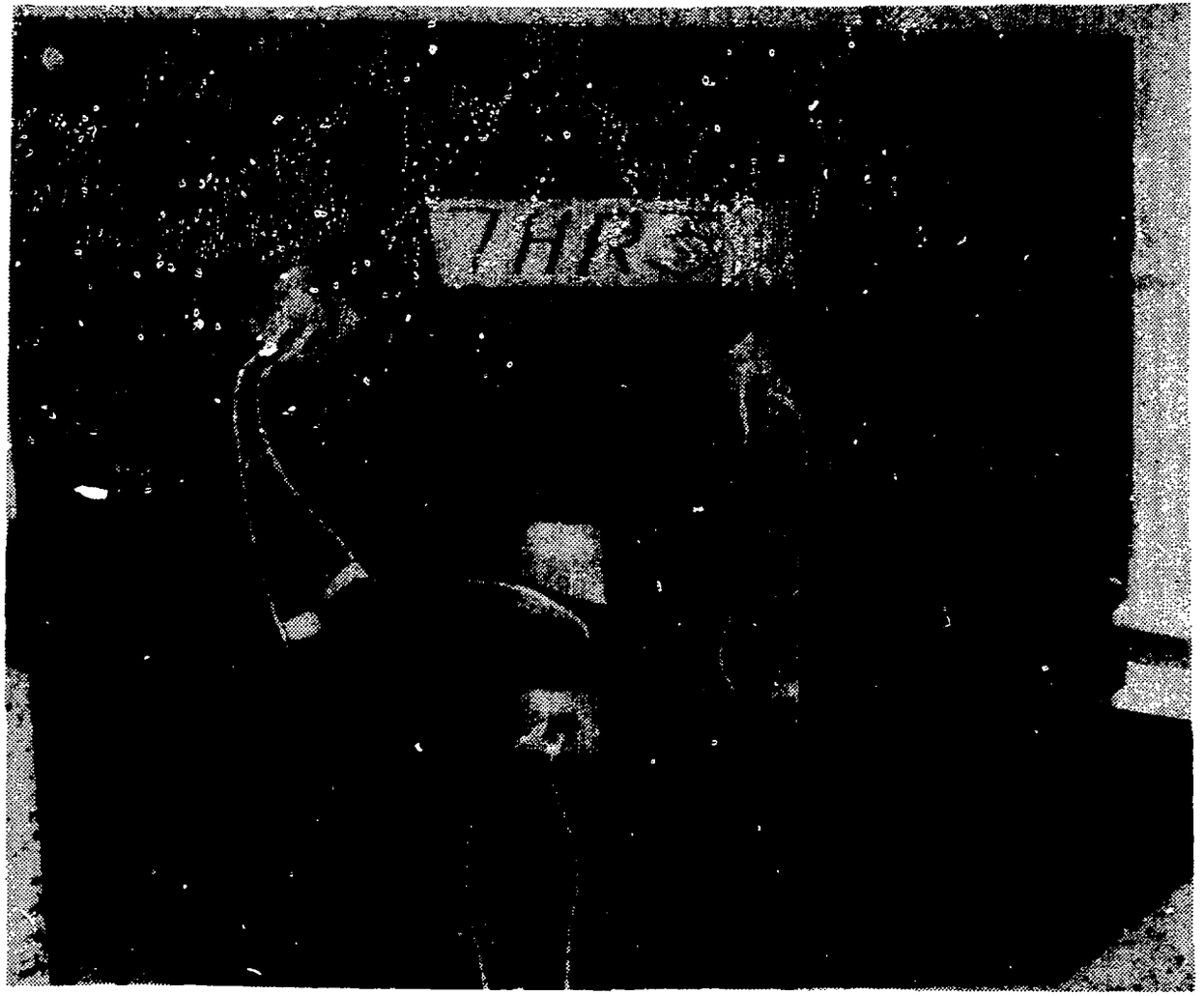

FIGURE 16. 7-HR-3 (Test Plate After Shot)

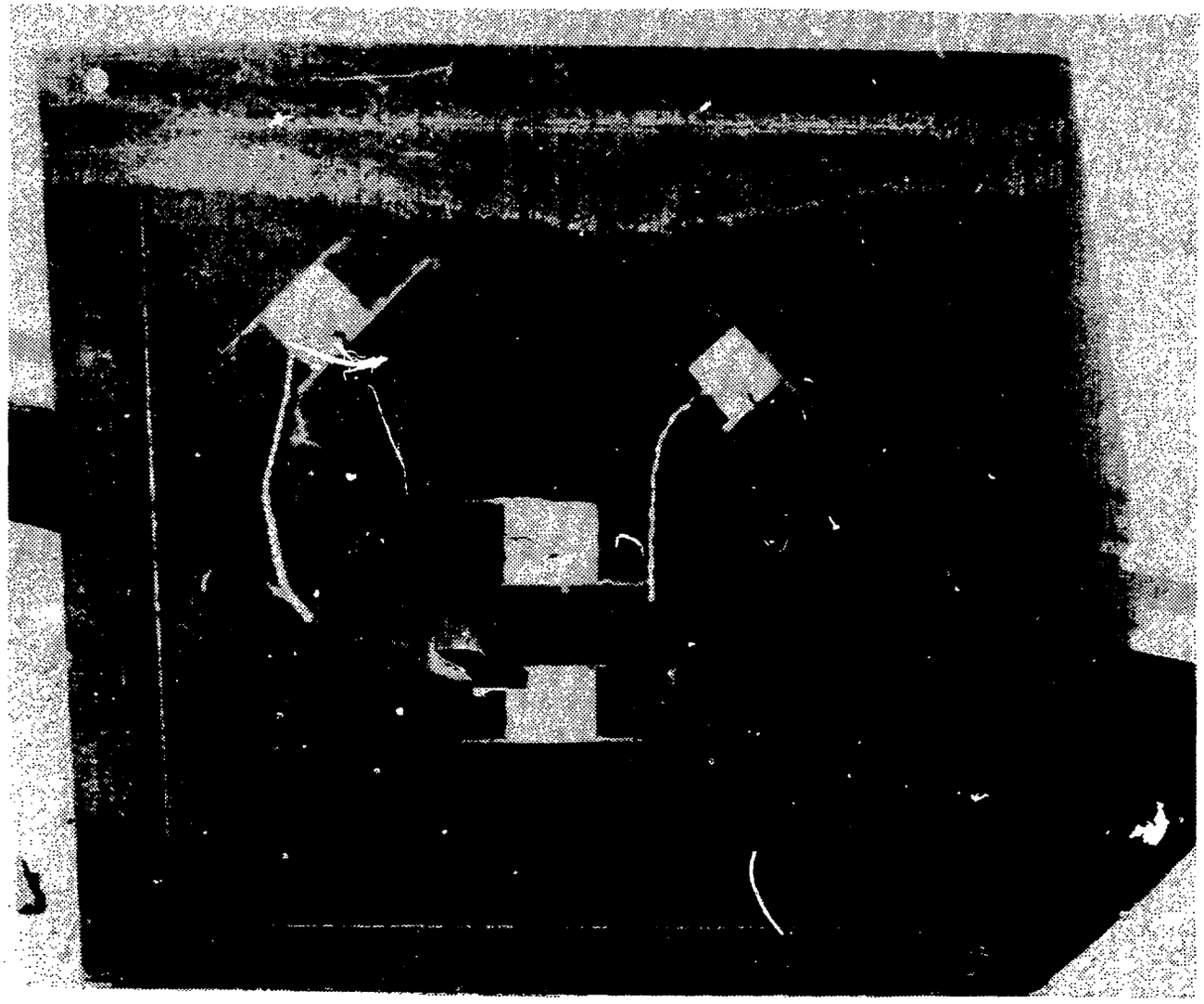

FIGURE 17. 7-HR-4 (Test Plate After Shot)

FIGURE 18. 7-HR-5 (Test Plate After Shot)

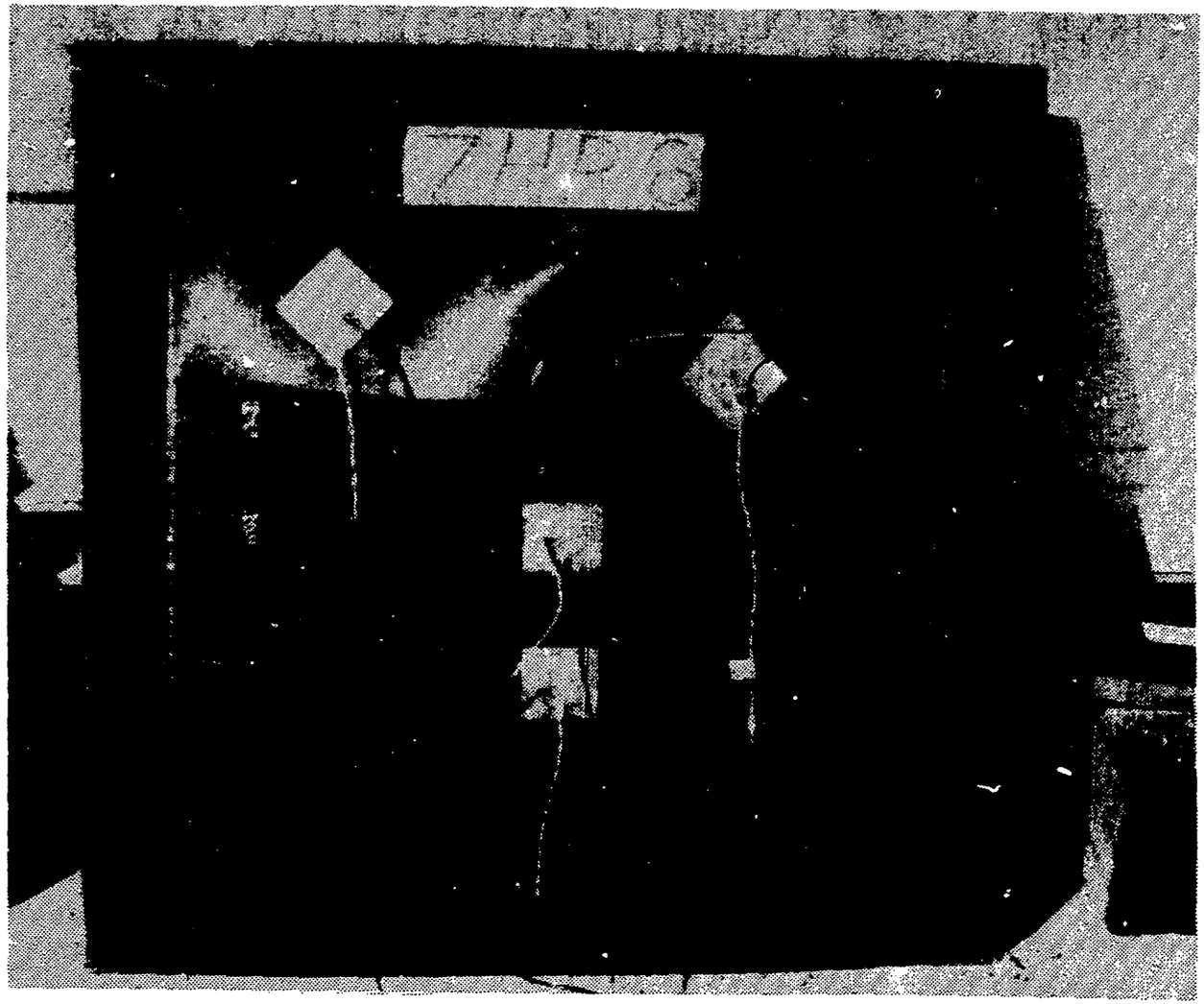

FIGURE 19. 7-HR-6 (Test Plate After Shot)

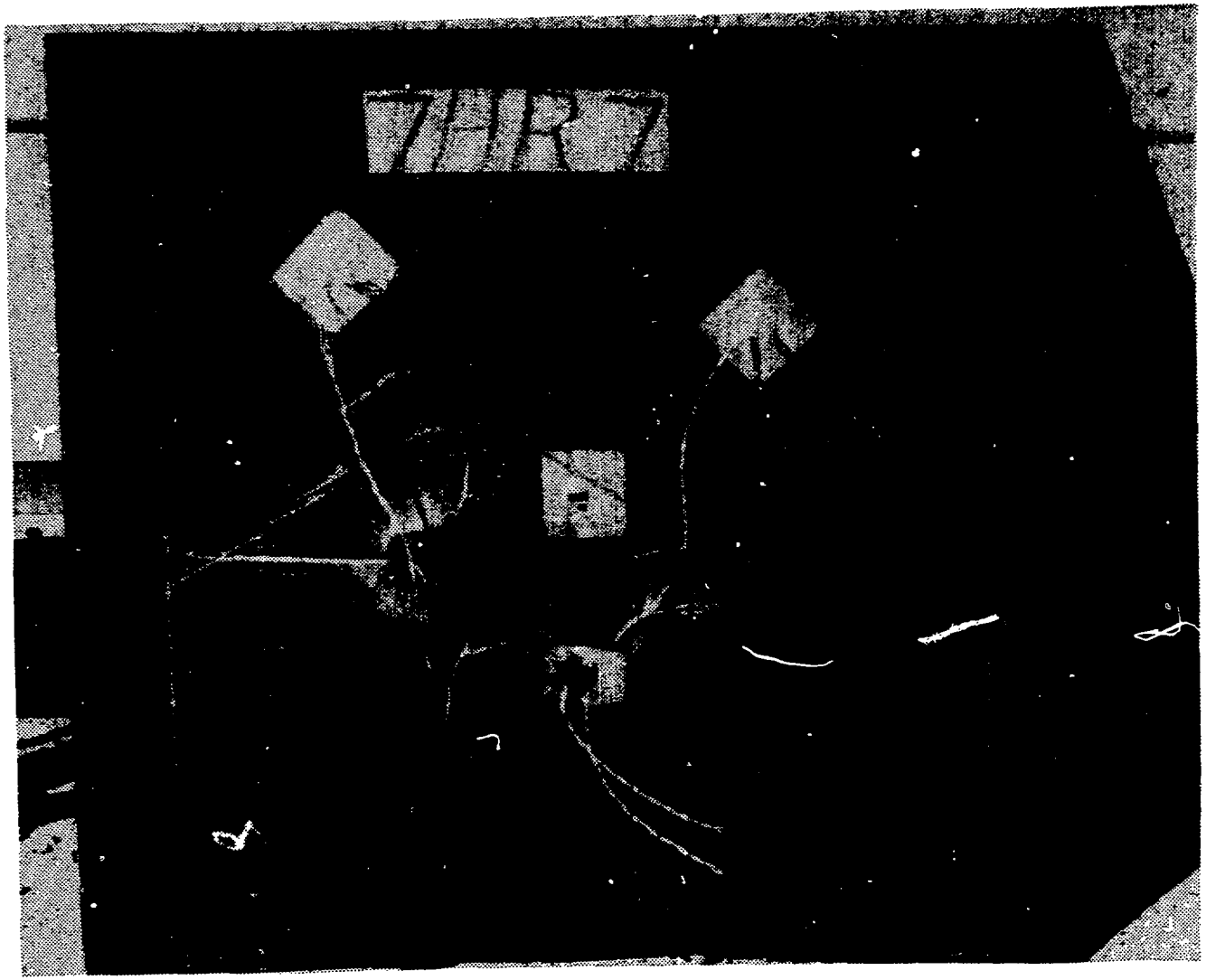

FIGURE 20. 7-HR-6 (Test Plate After Shot)

FIGURE 21. 7-HR-8 (Test Plate After Shot)

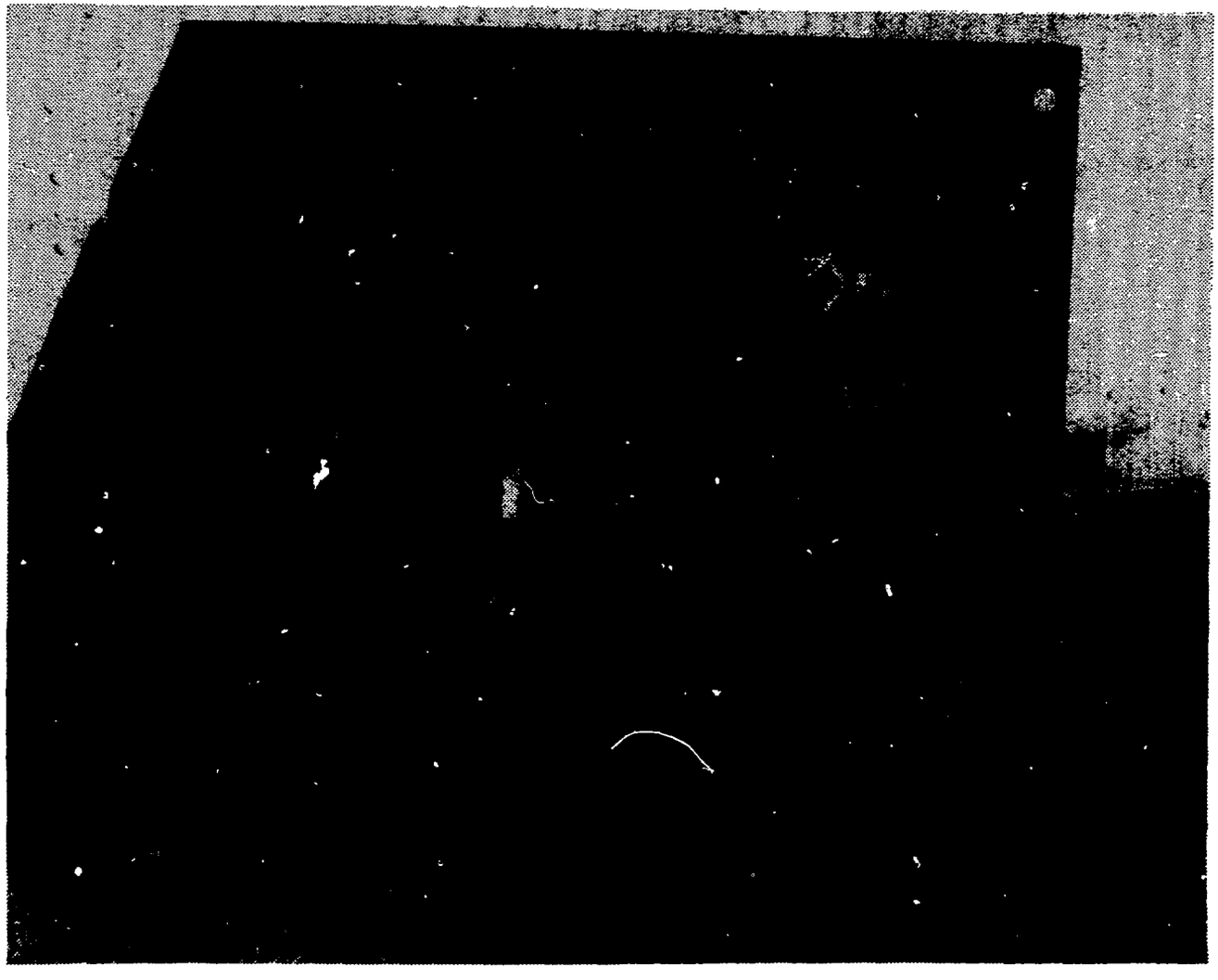

FIGURE 22. 7-HR-9 (Test Plate After Shot)

FIGURE 23. 7-HR-10 (Test Plate After Shot)

FIGURE 24. 7-HR-11 (Test Plate After Shot)

FIGURE 25. 7-HR-12 (Test Plate After Shot)

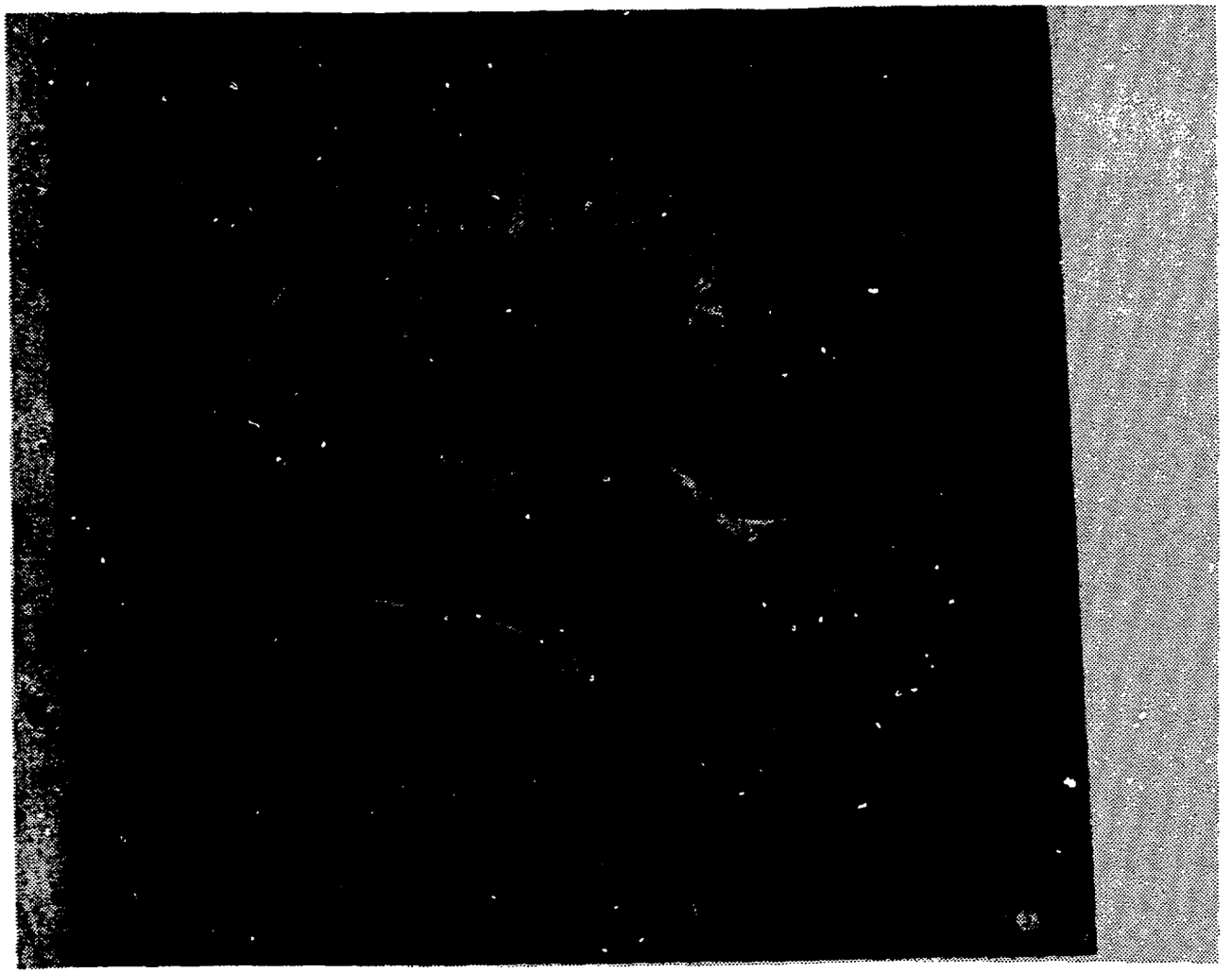

FIGURE 26. 7-HR-14 (Test Plate After Shot)

IV. FRACTOGRAPHIC EXAMINATION OF EXIT WALL FRACTURE SURFACE

One of the major objectives of this study was to determine the type of fracture caused by the hydraulic ram pressure loading, and if possible to determine the significance of strain rate effects on the fracture process. Consequently, a fractographic examination of the fracture surfaces of the NWC test plates was carried out. The photographs of the damaged plates, Figs. 14-26, and the actual NWC 7-HR-7 test plate were examined macroscopically, and various pieces of the fracture surfaces from the 7-HR-7 test plate were examined with the NPS scanning electron microscope (SEM).

A. MACROSCOPIC EXAMINATION

Examination of the fractures shown in Figs. 14-26 and the 7-HR-7 test plate showed that the fracture surfaces are generally slanted at approximately 45° to the plate surfaces. As described in Section II and shown in Fig. 10(a), this 45° slant of the fracture surface is characteristic of a relatively ductile fracture process of a thin plate in a plane stress condition. The 45° slant of the fracture surface is also an indication of a shear fracture, as described in Section II. The identification of the fractures as shear fractures was further strengthened by the fiborous, dull gray appearance of the 7-HR-7 test plate fracture surfaces.

B. SCANNING ELECTRON MICROSCOPE EXAMINATION

The examination of the fracture surfaces of the 7-HR-7 test plate with the SEM was considerably more complicated than the macroscopic examination. Figure 27 shows the locations on the 7-HR-7 test plate where the SEM specimens were taken. Figures 28-49 are the fractographs obtained using the SEM. As seen in Figs. 28-49, what appeared to be of uniform character to the unaided eye becomes extremely varied in nature when magnified 500 to 1200 times. These microfractographs have been compared to the microfractographs of 2024-T3, 2024-T4, and 7075-T6 aluminum shown in Ref. 29. The fractographs presented in Ref. 29 were obtained from samples fractured under very different circumstances than those of the 7-HR series, and are of different materials in some cases. Nevertheless, they are very similar to some of the fractographs presented here.

Figures 28-31 are SEM fractographs of specimen number 1. This specimen was obtained from location 1 shown in Fig. 27. This surface is where the projectile penetrated the plate. There were no fractographs in Ref. 29 similar to these four fractographs. Macroscopically this specimen appeared different from the others. The difference is probably due to the fact that the projectile penetrated the plate at this location. The surfaces shown in Figs. 28-31 appear to have been produced by a combination of fracture and scraping as the projectile penetrated the plate.

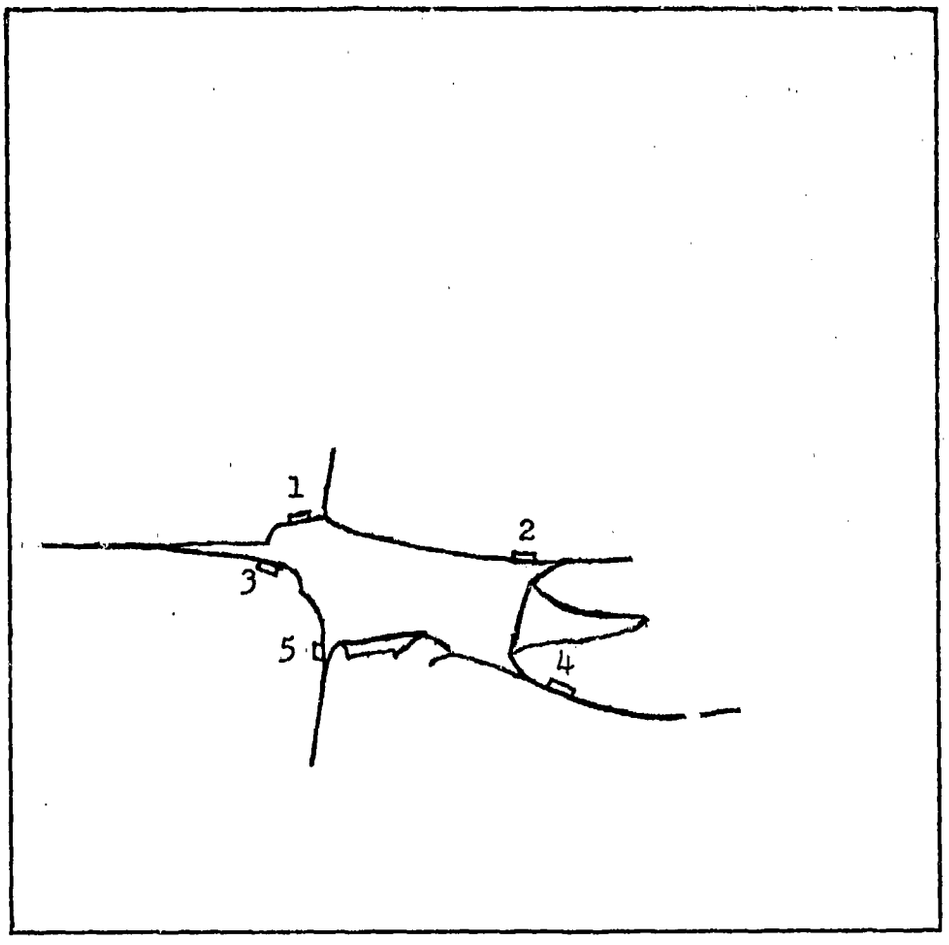

FIGURE 27. Location of SEM Specimens on 7-HR-7 Test Plate

FIGURE 28. SEM Fractograph of Specimen #1 x620

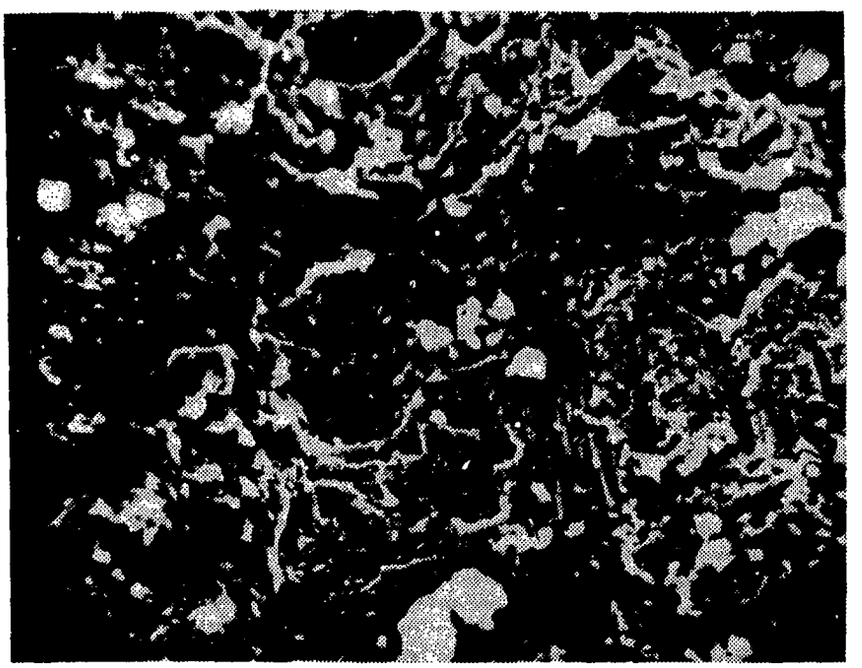

FIGURE 29. SEM Fractograph of Specimen #1 x600

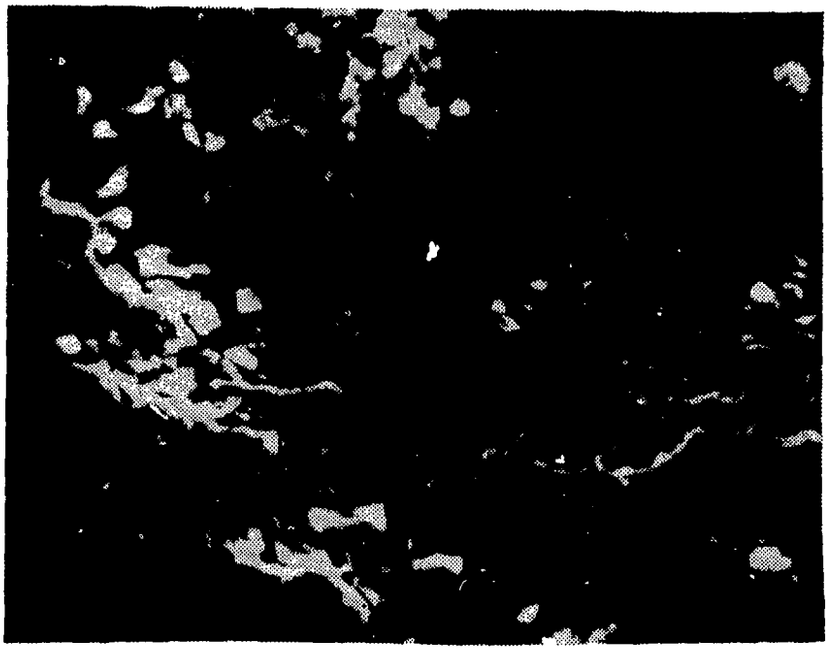

FIGURE 30. SEM Fractograph of Specimen #1 x640

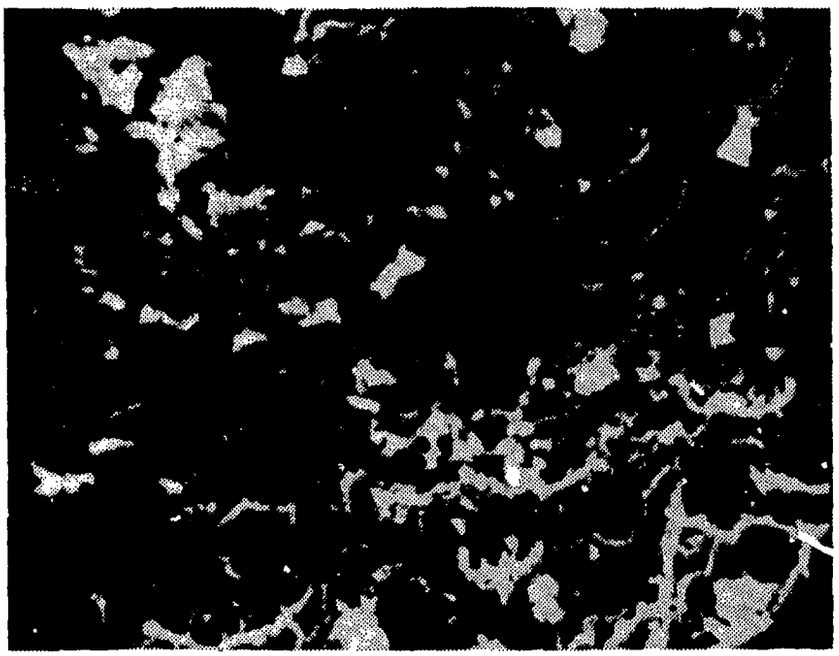

FIGURE 31. SEM Fractograph of Specimen #1 x650

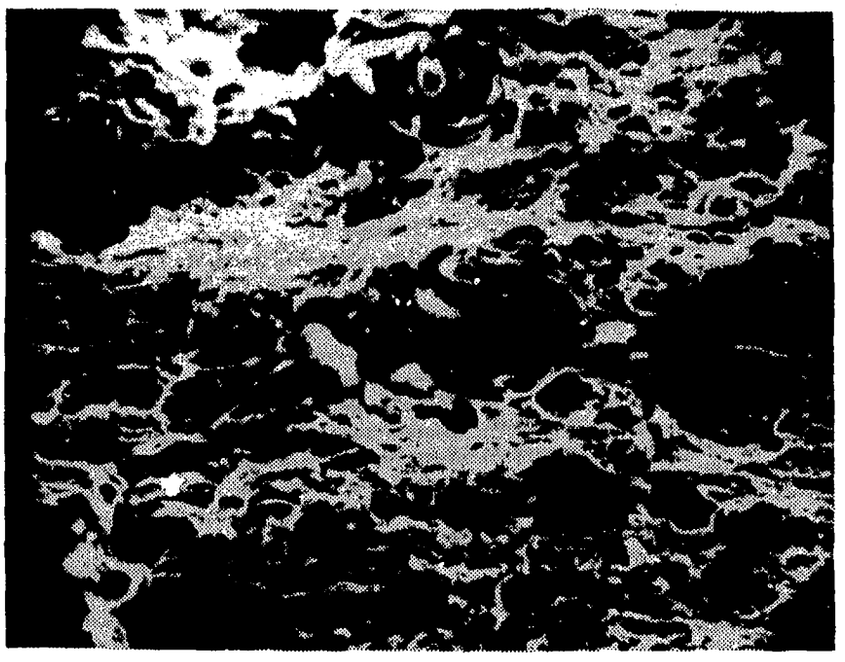

FIGURE 32. SEM Fractograph of Specimen #2 x560

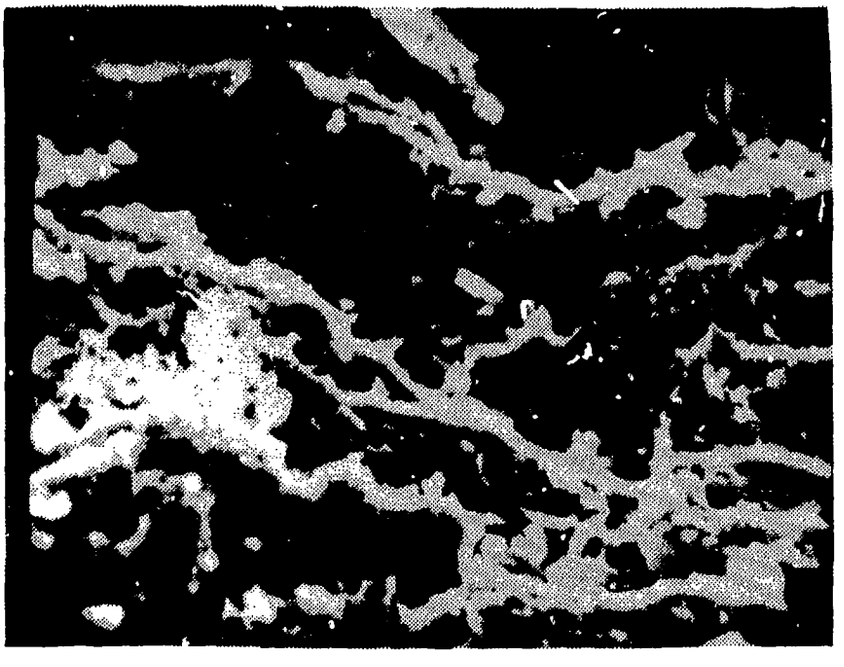

FIGURE 33. SEM Fractograph of Specimen #2 x1100

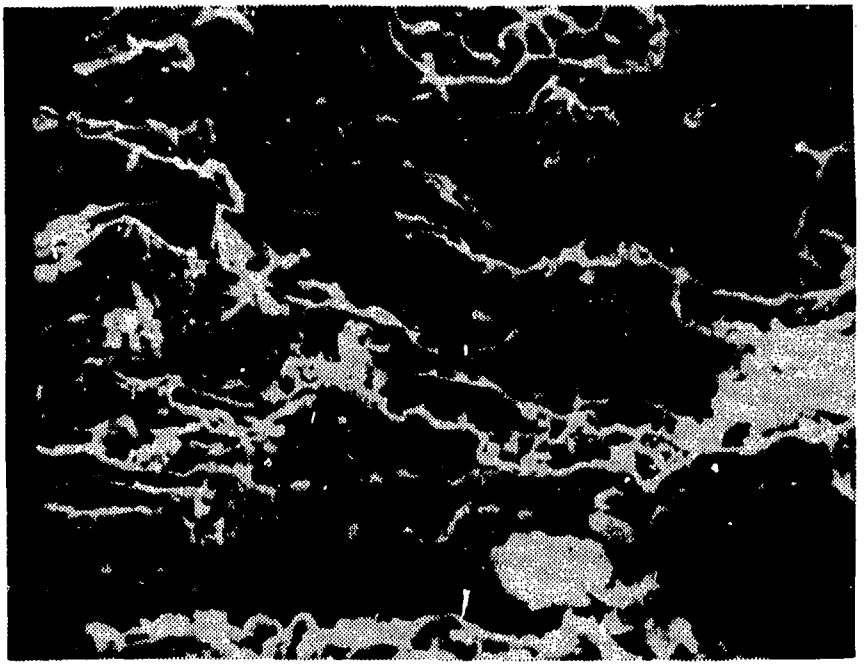

FIGURE 34. SEM Fractograph of Specimen #2 x550

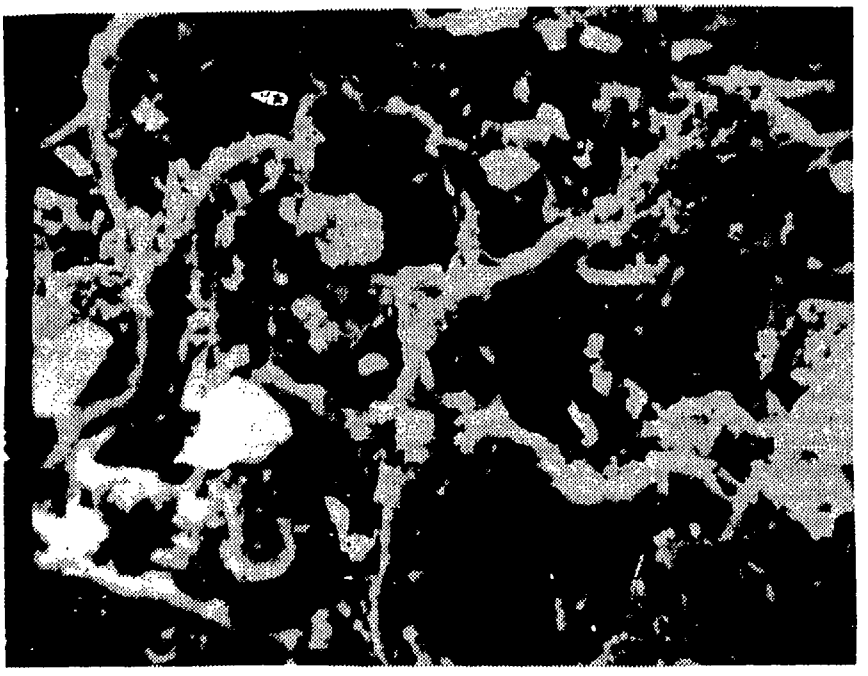

FIGURE 35. SEM Fractograph of Specimen #2 x1100

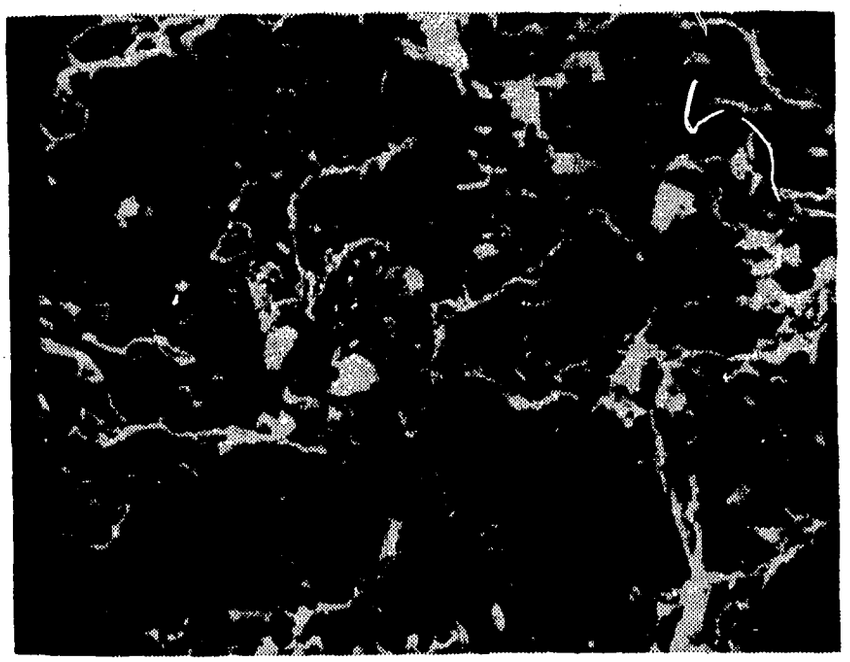

FIGURE 36. SEM Fractograph of Specimen #2 x550

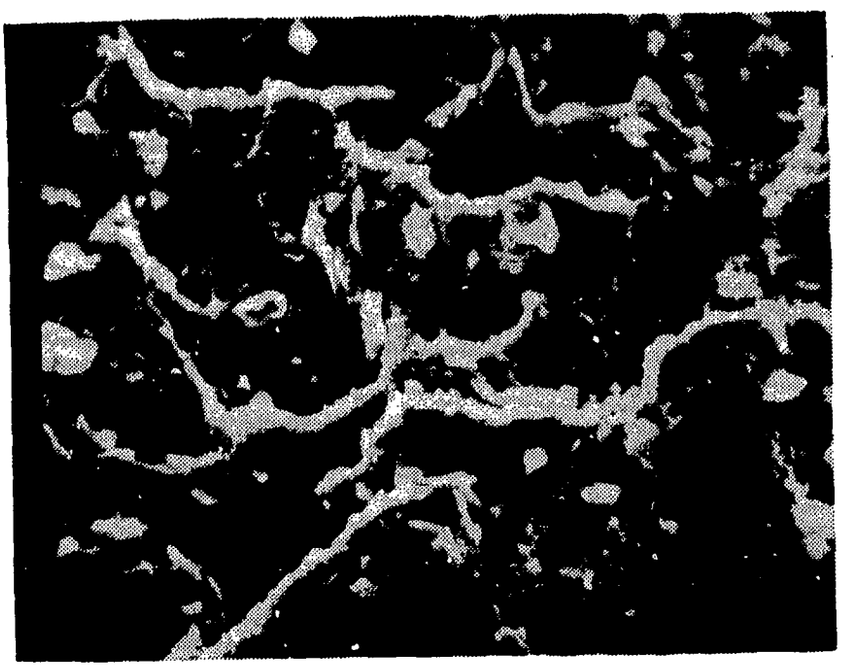

FIGURE 37. SEM Fractograph of Specimen #2 x1100

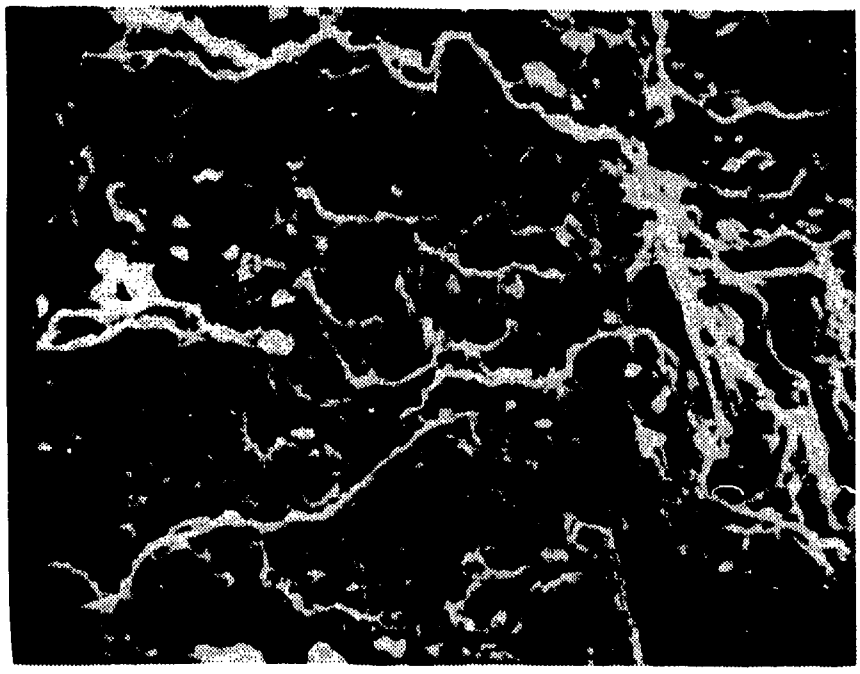

FIGURE 38. SEM Fractograph of Specimen #2 x550

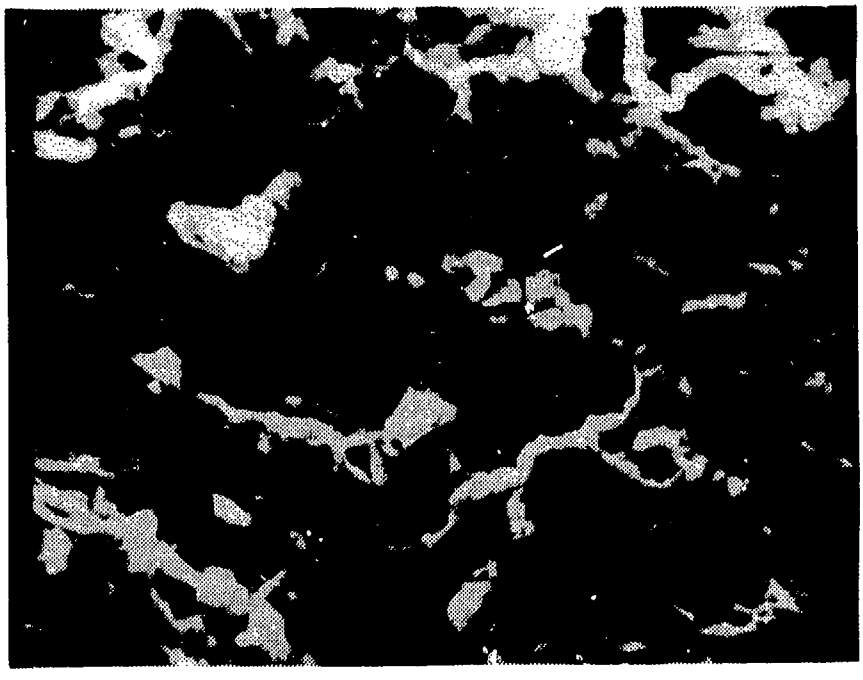

FIGURE 39. SEM Fractograph of Specimen #4 x1200

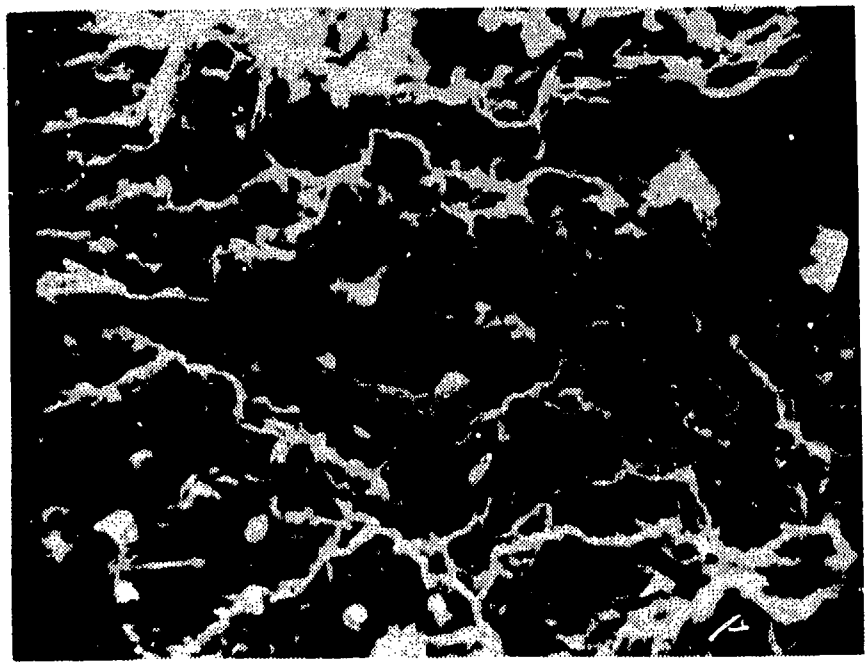

FIGURE 40. SEM Fractograph of Specimen #4 x600

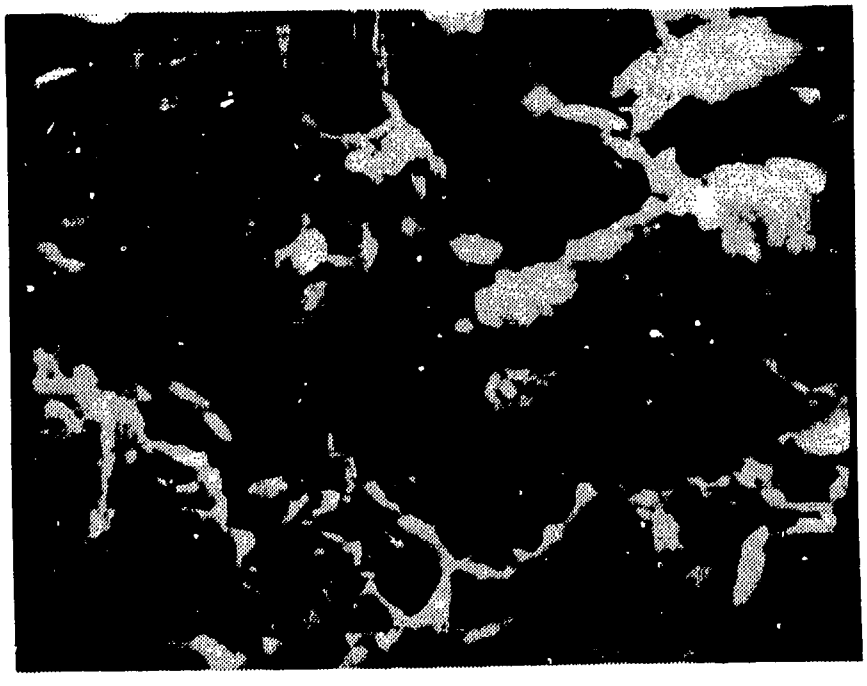

FIGURE 41. SEM Fractograph of Specimen #4 x1250

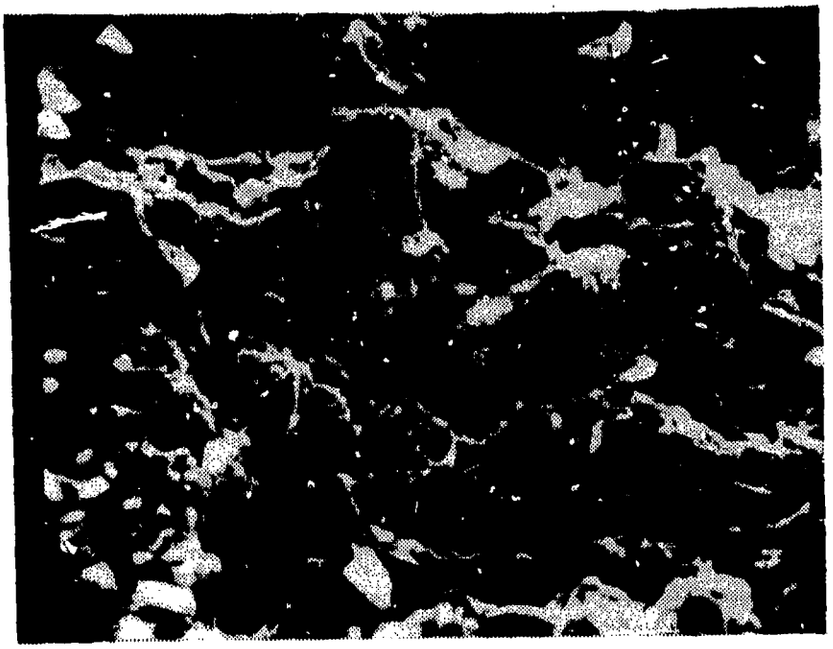

FIGURE 42. SEM Fractograph of Specimen #4 x625

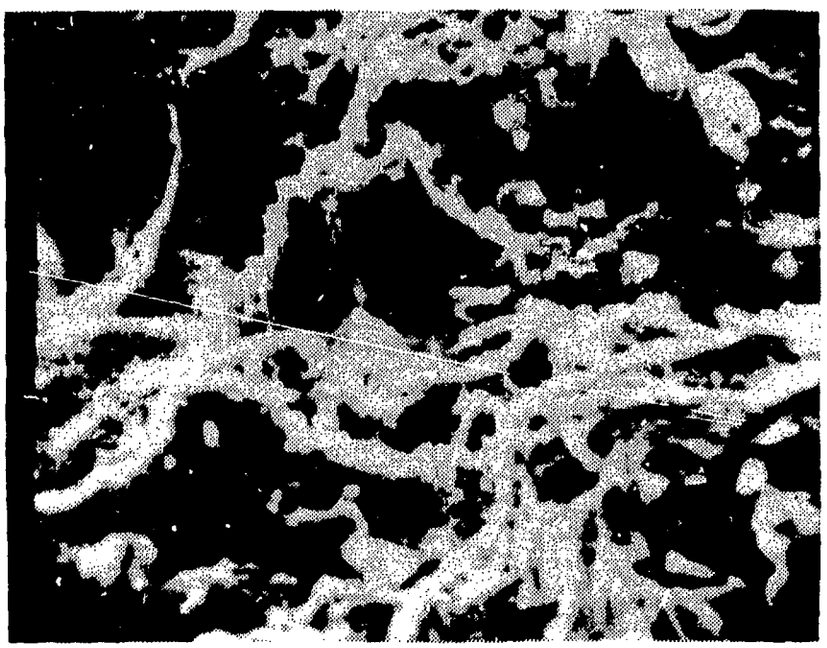

FIGURE 43. SEM Fractograph of Specimen #5 x1200

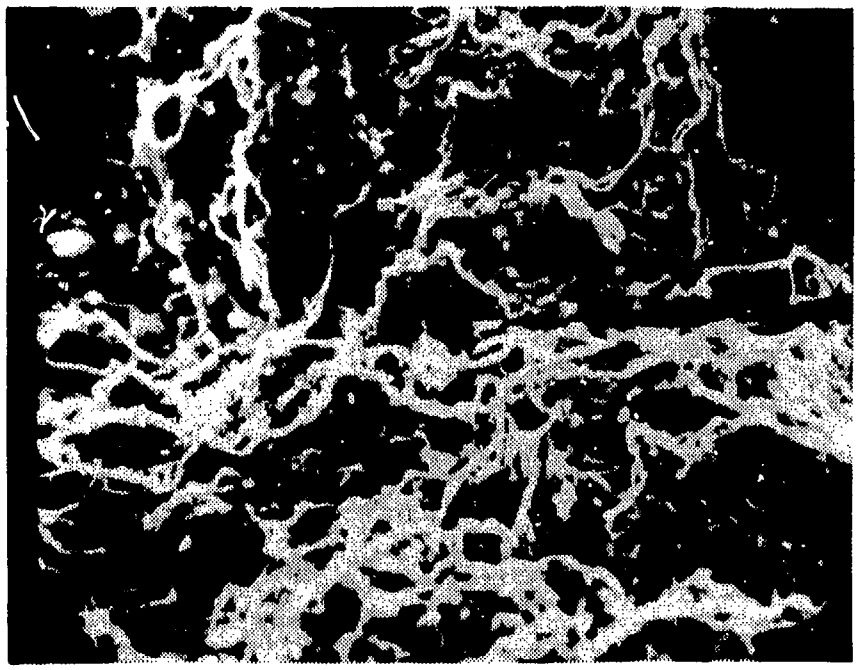

FIGURE 44. SEM Fractograph of Specimen #5 x600

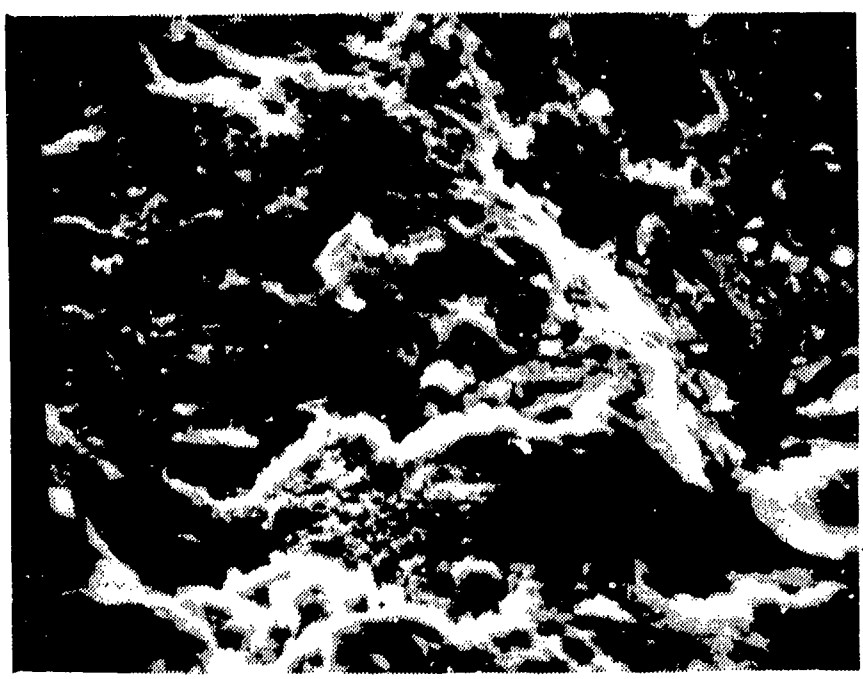

FIGURE 45. SEM Fractograph of Specimen #5 x1100

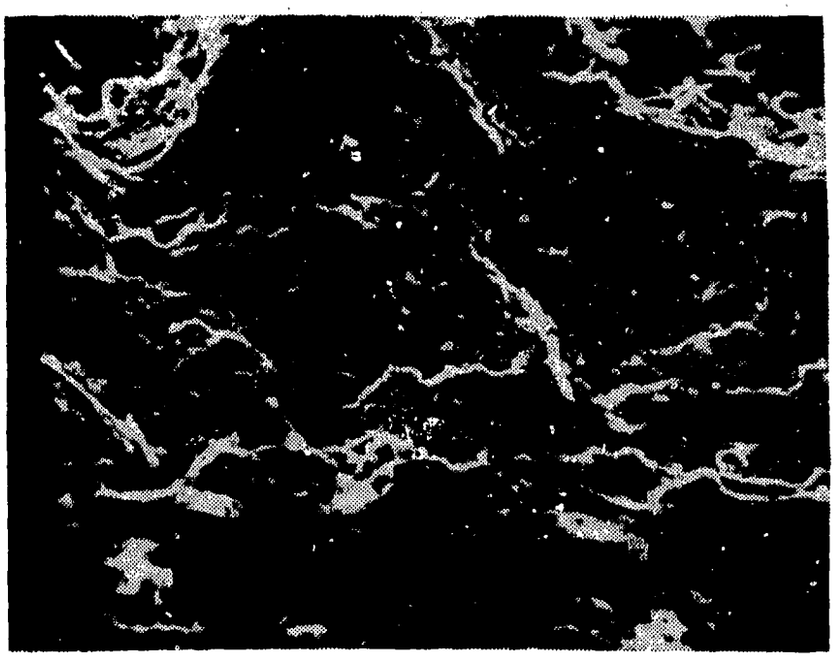

FIGURE 46. SEM Fractograph of Specimen #5 x550

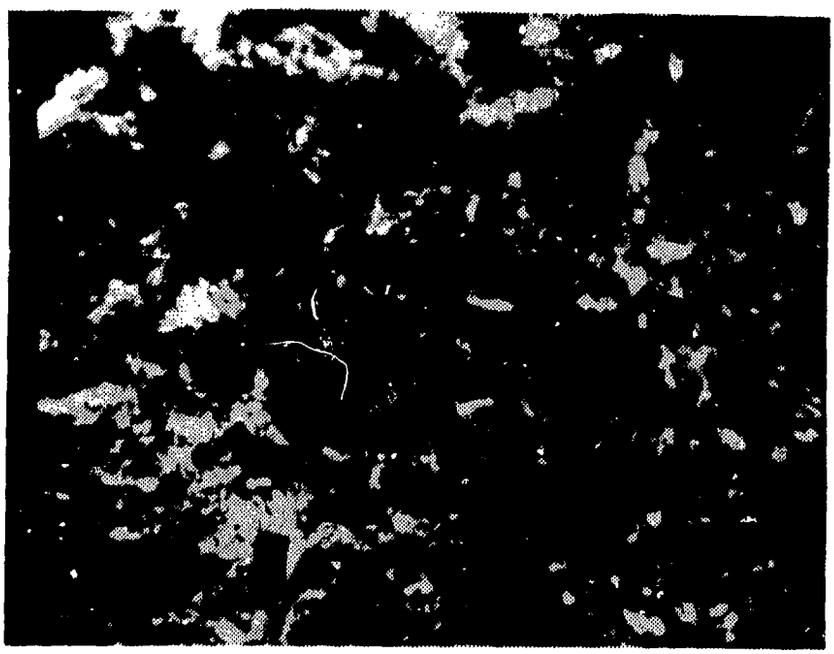

FIGURE 47. SEM Fractograph of Specimen #3 x1200

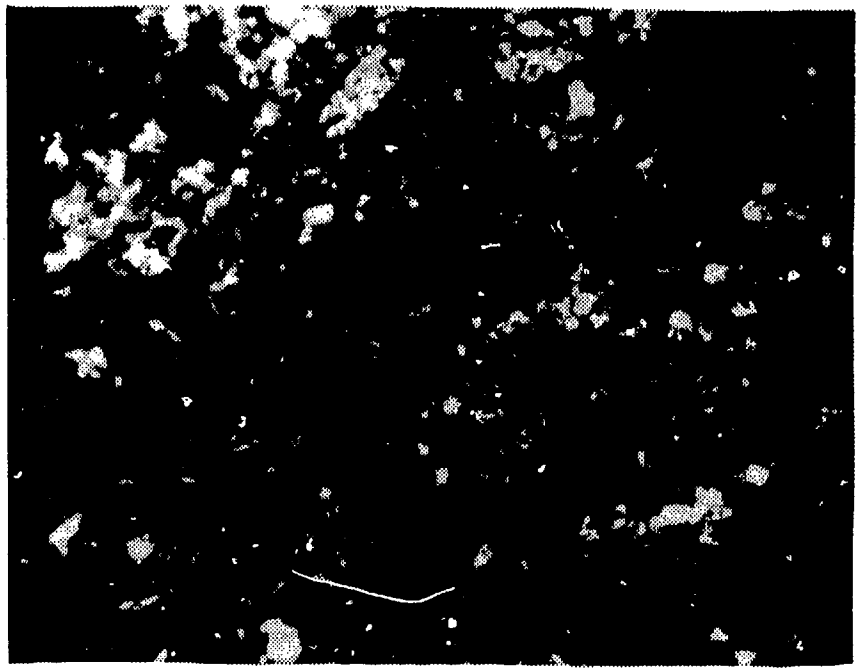

FIGURE 48. SEM Fractograph of Specimen #3 x1150

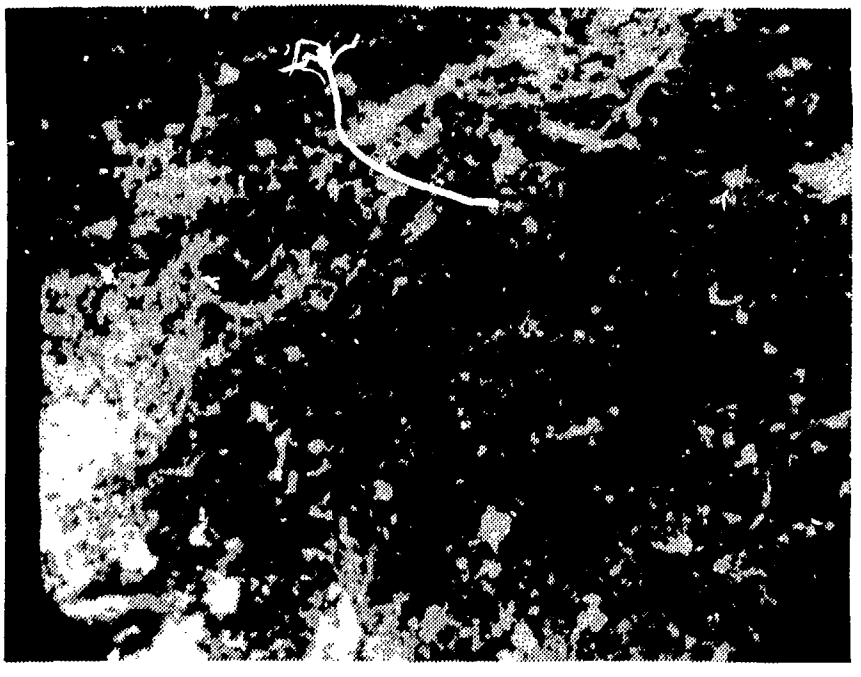

FIGURE 49. SEM Fractograph of Specimen #3 x575

Figures 32-46 are SEM fractographs of specimens 2, 4, and 5, as indicated in the captions. These figures are similar enough to be considered together. These figures were compared with Figs. 4022, 4023, and 4028 of Ref. 29 and that portion of Ref. 29 entitled "Interpretation of Scanning-Electron-Microscope Fractographs." Most of the surfaces of the specimens are composed of dimples formed by microvoid coalescence with tear ridges. The dimples are indicative of a shear type fracture with the dimples and tear ridges also indicating a ductile process. Some of the large smooth areas, such as those in Figs. 35, 37, and 43, could possibly be cleavage or intercrystalline fractures, but these areas are believed to be the result of microvoid surfaces that have been stretched. The elimination of the possibility of cleavage fracture seems justified due to the lack of river patterns in the large smooth areas which are characteristic of cleavage fractures. The elimination of the possibility of intercrystalline fracture seems justified due to the lack of intergranular secondary fissures such as shown in Fig. 4028 of Ref. 29.

Figures 47-49 are SEM fractographs of specimen 3 which, like specimen 1, came from very close to the projectile penetration point. The surface represented by these fractographs could not be characterized into a definite pattern, although there is an indication of some dimpling.

C. HIGH SPEED MOTION PICTURES

High speed motion pictures taken of the 7-HR series tests showed lapsed time from projectile penetration of the plate until the cracks stopped increasing of between 0.625 and 2.0 msec. The longer times were associated with the 7-HR high velocity, high damage shots 6-9, and the shorter times were associated with the 7-HR low velocity shots 10-14. The high speed films are discussed in more detail in Section V.

V. EXIT WALL CRACK LENGTH ANALYSIS AND RESULTS

The second major objective of this study was to develop a macroscopic method for predicting the extent of cracking in the exit wall of a fuel tank due to hydraulic ram. Shots 10, 11, 12, and 14 of the NWC 7-HR series tests were used in the development of the proposed prediction method because of their low velocity and the relatively minor damage they caused. The method of crack length prediction follows.

Computer codes for the fluid pressure and the structural response are used to predict the stresses in the exit wall. A correction factor, determined as explained later in this section, is applied to the predicted stresses. The corrected stresses are plotted as a function of the distance from the projectile penetration point. Reference is made to empirical data to find the stress required to increase the crack length for various initial crack lengths. The stress required to increase the crack length is plotted as a function of the crack length on the same graph as the corrected stresses. Thus, the predicted crack length is that crack length at which the corrected stress first falls below the stress required for crack extension.

A. ANALYSIS FOR MAXIMUM PREDICTED WALL STRAINS AND A COMPARISON WITH EXPERIMENTAL DATA

The NWC digital computer program for the hydraulic ram wall pressures, as described in Ref. 5, and SATANS, as modified

in Ref. 24, have been used to predict the axi-symmetric strains in the exit wall on a radial line at one-half inch intervals. In the analysis, the projectile penetration point was assumed to be at the center of the plate, as shown in Fig. 50. SATANS was used for the analysis of the rectangular wall instead of BR-1HR because its computer execution time is considerably less than that of BR-1HR, which takes several hours of IBM 360/67 execution time for a typical solution using a coarse model. The parameters used in the two computer codes were those of the NWC 7-HR-14 test, which is similar enough to the 7-HR-10, 11, and 12 shots to make the results comparable for any of the four tests. Piston theory was used to approximate the fluid-structure interaction. Cavitation at the exit wall was assumed if the net interface pressure between the fluid and wall became negative (tension). The results of the computer analysis are compared with the experimentally measured strains in Ref. 25.

According to Ref. 25, the magnitudes of the strains predicted by the computer analysis do not agree very closely with the actual strains measured in the NWC 7-HR series experiments. Figures 51-56 are graphs of the actual strains measured by the strain gages located as shown in Fig. 13 and of the predicted strains at the point marked A in Fig. 13 and Fig. 50. Figures 51, 52, and 55 are the strains, actual and predicted as indicated, in the y-direction. Figures 53, 54, and 56 are the strains, actual and predicted as indicated, in the x-direction.

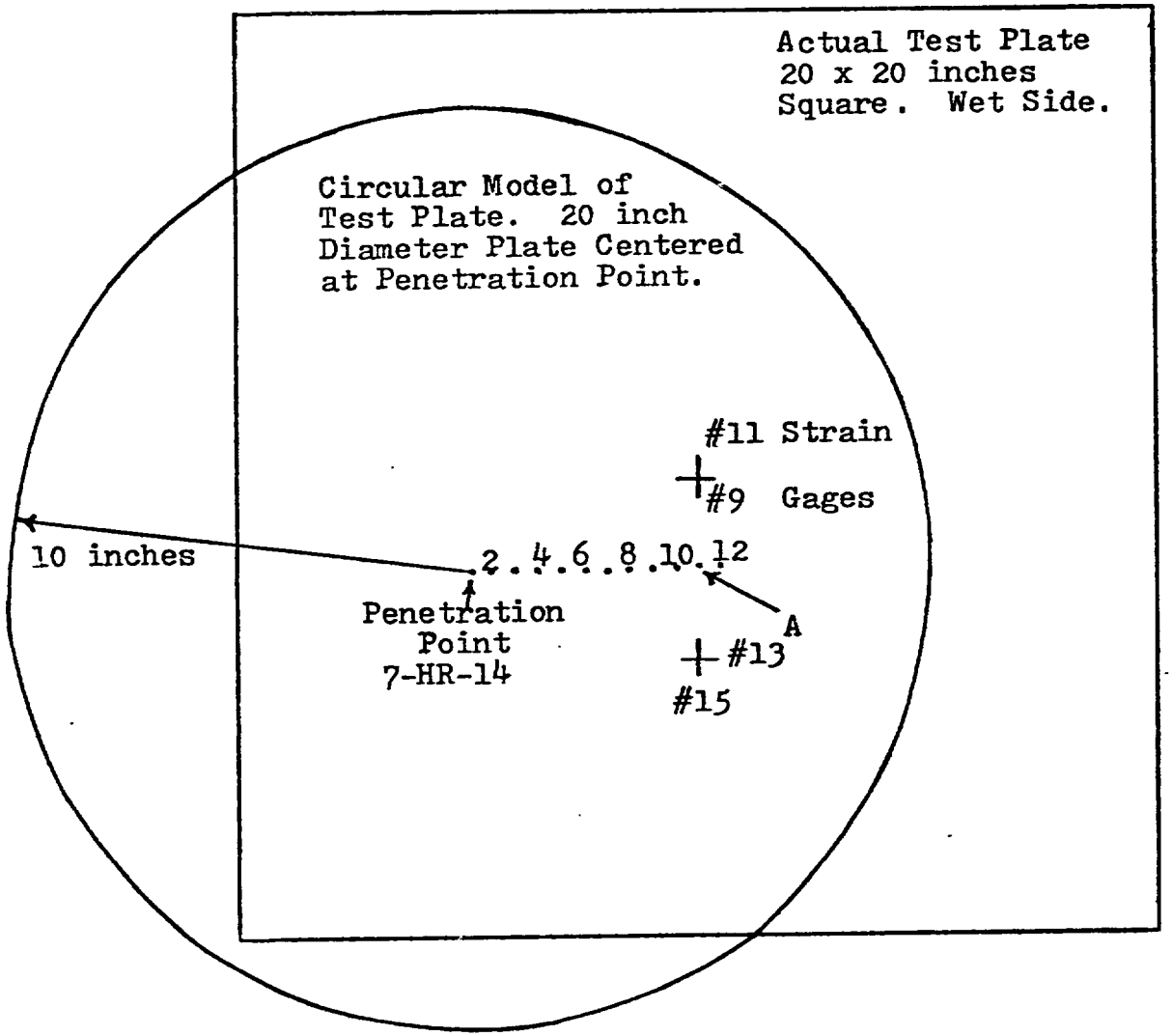

FIGURE 50. Test Plate Model Superimposed on Actual Test Plate

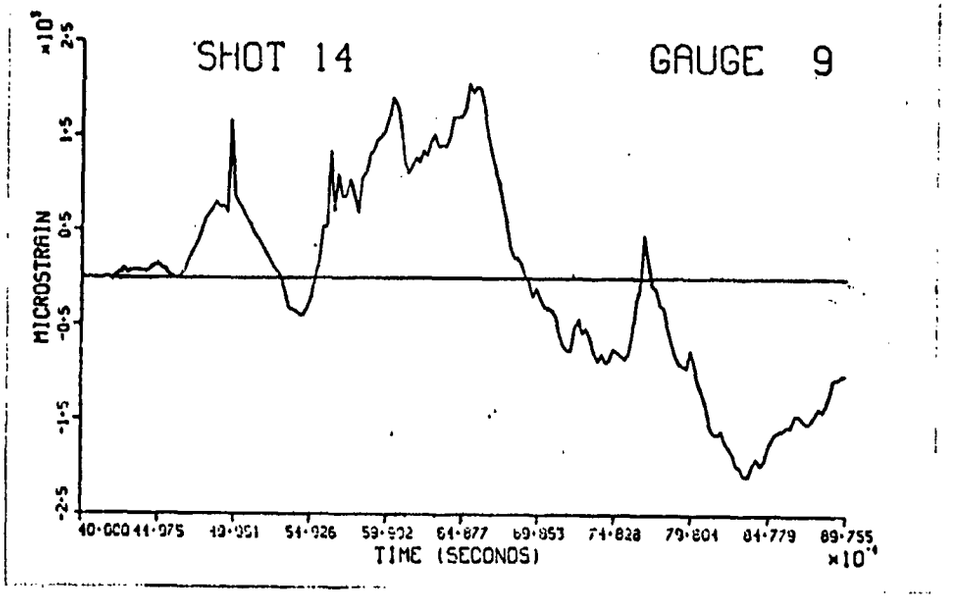

FIGURE 51. Strains Measured by Gage 9 in 7-HR-14 Shot

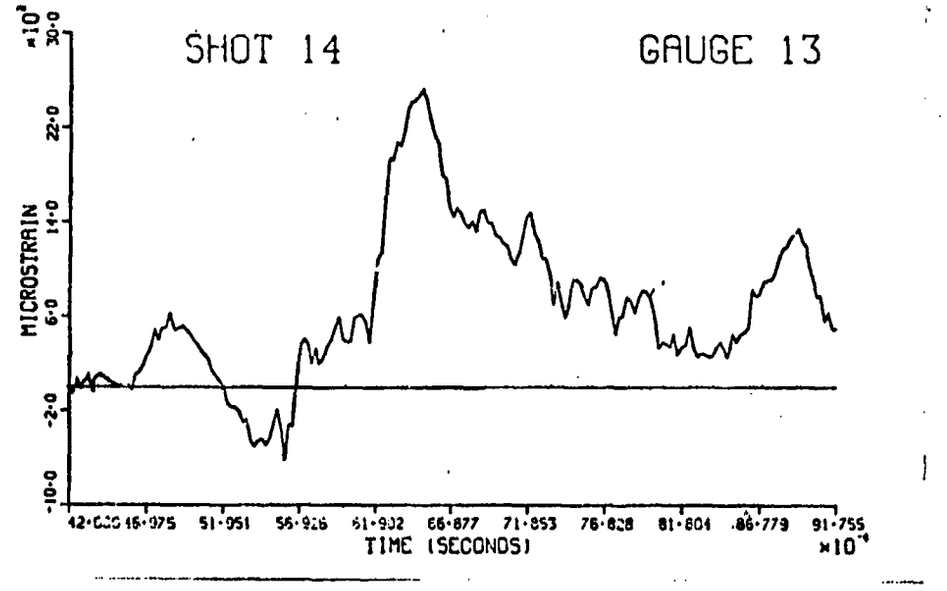

FIGURE 52. Strains Measured by Gage 13 in 7-HR-14 Shot

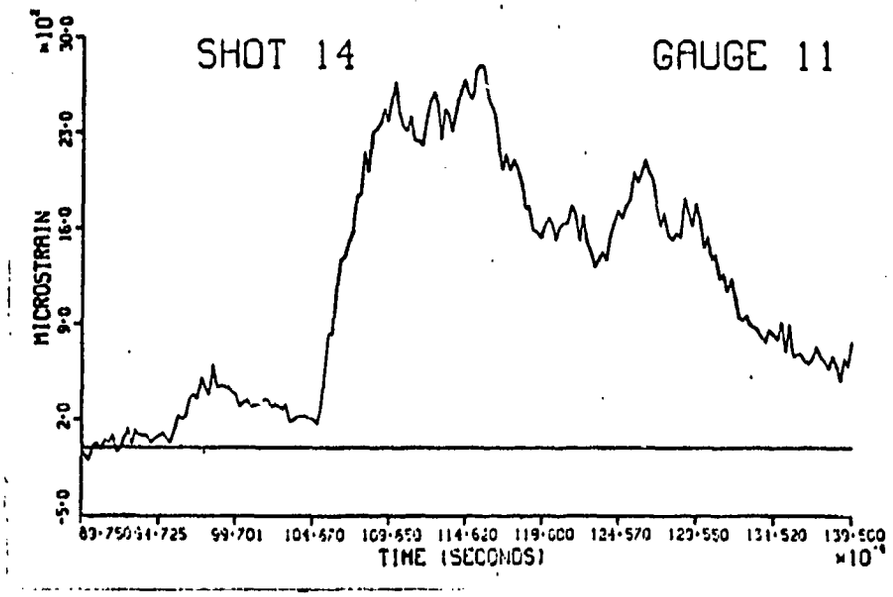

FIGURE 53. Strains Measured by Gage 11 in 7-HR-14 Shot

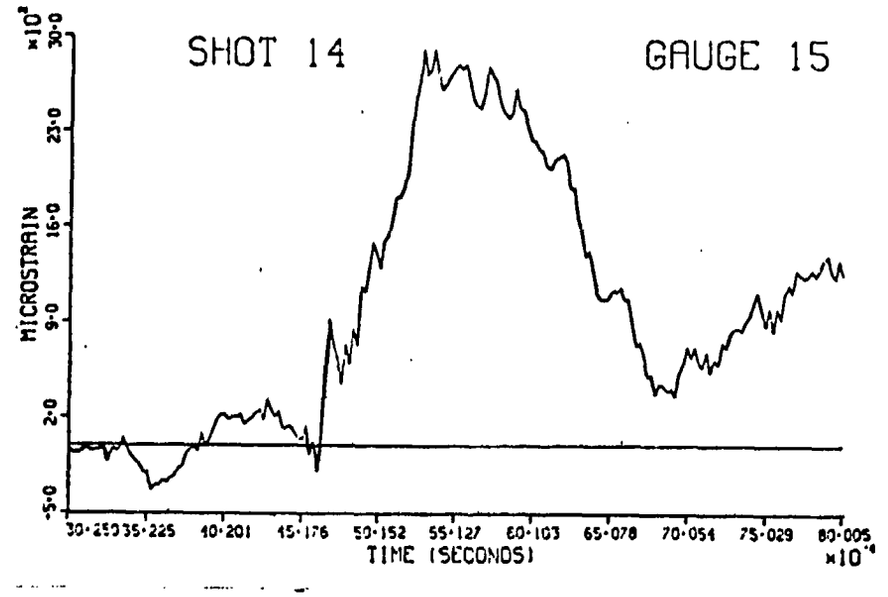

FIGURE 54. Strains Measured by Gage 15 in 7-HR-14 Shot

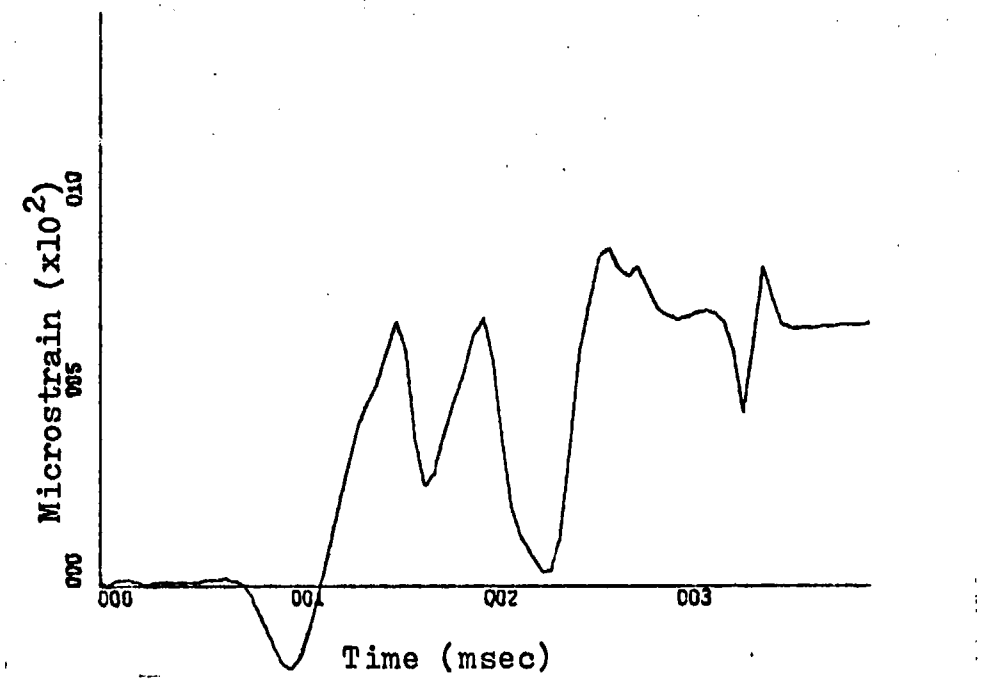

FIGURE 55. y-direction Strains Predicted by SATANS at Point "A" for 7-HR-14 Shot

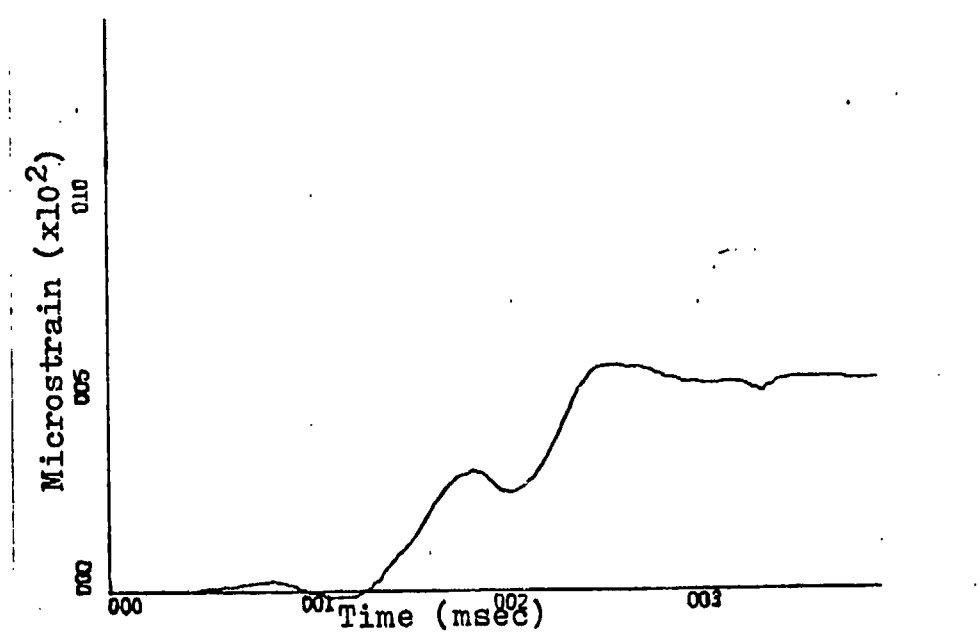

FIGURE 56. x-direction Strains Predicted by SATANS at Point "A" for 7-HR-14 Shot

Although the magnitudes of the actual strains are much larger than the predicted strains, the basic shape of the corresponding strain histories are roughly similar.

The maximum predicted strains at point A have been compared with the average of the maximum strains recorded on the corresponding strain gages at the two locations. The comparison showed that the x-direction predicted strains were low by a factor of 4.6 and the y-direction predicted strains were low by a factor of 2.4. One reason for the difference in correction factors could be that SATANS analyzes a circular plate with the penetration point at the center, while the actual plate is square with the penetration point located off center as shown in Fig. 50. In addition, the actual locations of the strain gages do not correspond exactly to the location of the predicted strains. Other possible reasons are that the method used to treat the fluid-structure interaction, the assumption of cavitation, and the hydraulic ram pressure analysis are not representative of the actual situation. A further discussion of the comparison is given in Ref. 25.

The predicted strains were used to determine the stresses σ_x and σ_y on the outside surface of the tank exit wall (dry), with σ_x aligned circumferentially and σ_y aligned radially. The maximum positive σ_x and σ_y stress predicted by SATANS at stations 2 thru 12 (representing 0.5 to 5.5 inches from the penetration point) are presented in Table IV and plotted in Figs. 57 and 58. Table IV also shows the σ_x on the inside surface of the tank exit wall (wet) at the same time that

TABLE IV

Data Predicted by SATANS

Station	Distance From Exit Point (inches)	Time Max $\sigma_{x,y}$ Reached ($\times 10^{-3}$ sec)	σ_x max dry (ksi)	σ_x wet (ksi)	σ_y max dry (ksi)
2	0.5	2.1	14.38	-10.36	19.11
3	1.0	2.15	16.30	- 8.95	18.04
4	1.5	2.2	14.86	- 7.74	15.78
5	2.0	2.25	12.99	- 6.32	13.58
6	2.5	2.25	11.29	- 5.50	10.28
7	3.0	2.4	10.16	- 3.51	12.26
8	3.5	2.45	10.11	- 3.55	12.79
9	4.0	2.55	10.07	- 3.21	13.04
10	4.5	2.55	9.83	- 3.66	12.37
11	5.0	2.65	9.36	- 3.33	11.61
12	6.0	2.7	8.65	- 3.17	10.39

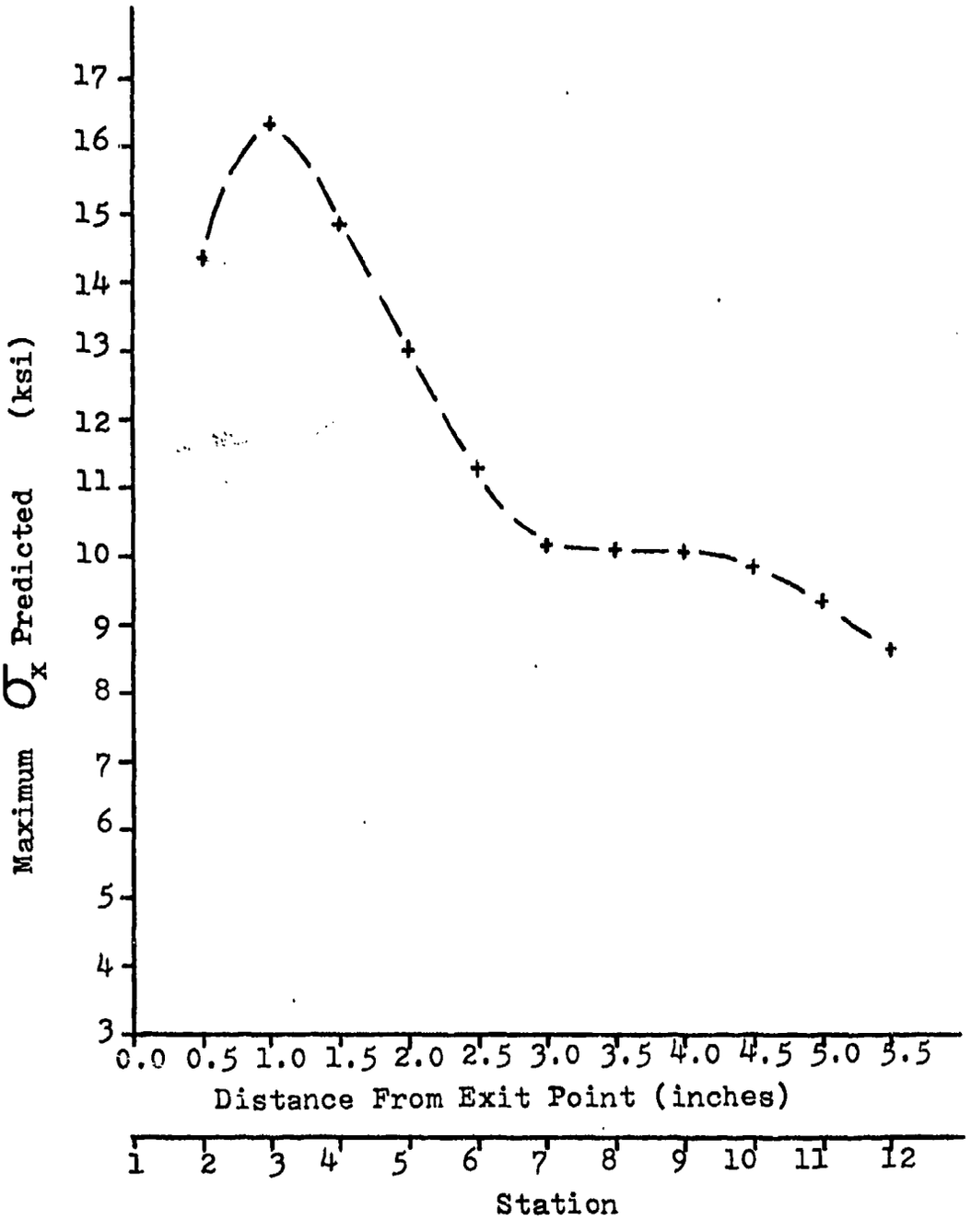

FIGURE 57. Maximum Stress σ_x predicted by SATANS on the dry side of the plate plotted against distance from exit point.

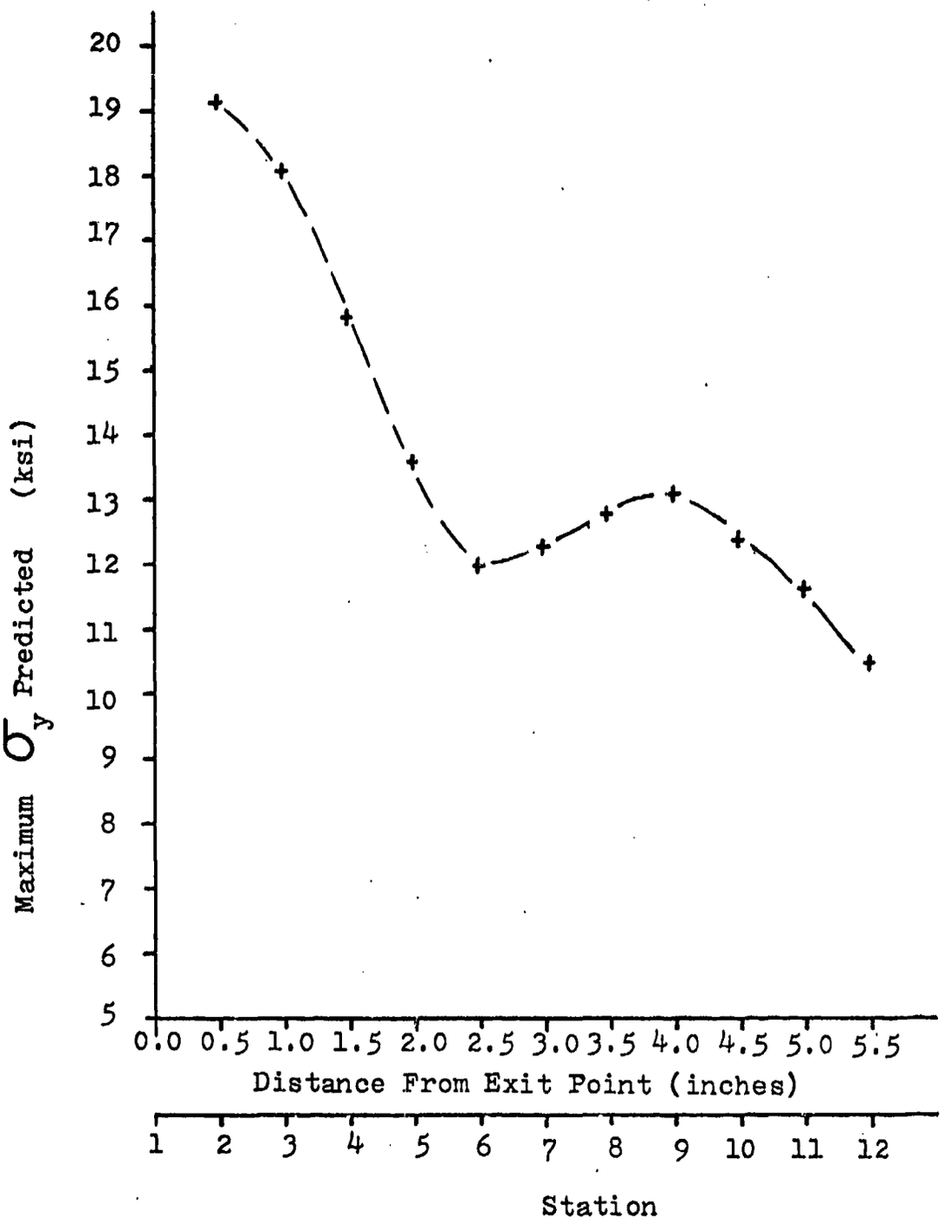

FIGURE 58. Maximum Stress σ_y predicted by SATANS on the dry side of the plate plotted against distance from exit point.

the other stresses were measured. By comparing σ_x dry to σ_x wet, a profile of the stress through the plate thickness may be obtained. This profile reveals that significant stretching of the plate is predicted. Further examination of Table IV shows that the maximum stress predicted starts at station 2 and proceeds sequentially with time outward to station 12. Since the maximum stress around a crack is normally at the crack tip, the predicted succession of maximum stresses moving outward from the center seems consistent with the idea of a crack growing from the penetration point outward toward the edge of the plate.

B. PROCEDURE FOR PREDICTING THE MAXIMUM CRACK LENGTH

Because the fracture surfaces of the actual test plates appear similar to simple tensile tests of thin plate specimens, tensile test data from the stretching of cracked plates was examined. For example, analysis of the data presented in Table CAD10 of Ref. 34 reveals a pattern in the fracture of 0.125 inch thick 2024-T3 aluminum cracked plates. For test specimens of width 4, 8, and 24 inches, the stress required to cause a crack to increase in length was found to be a function only of the ratio of specimen width to crack length. The correspondence between the fracture stress and the ratio is shown in Table V and plotted in Fig. 59.

Table VI shows the approximation made to the crack length data of Table II in order to obtain a single straight crack of equal damage to the small multiple cracks of the 7-HR series

TABLE V

Stress Required to Increase Crack Length in 2024-T3 Tensile Specimens [34]

Specimen Width	Specimen Width to Crack Length Ratio	max
4 inch	10/1	46
4 inch	10/3	36
4 inch	10/6	20
8 inch	10/1	46
8 inch	10/3	34
8 inch	10/6	20
12 inch	10/1	45
12 inch	10/3	29
12 inch	10/6	17

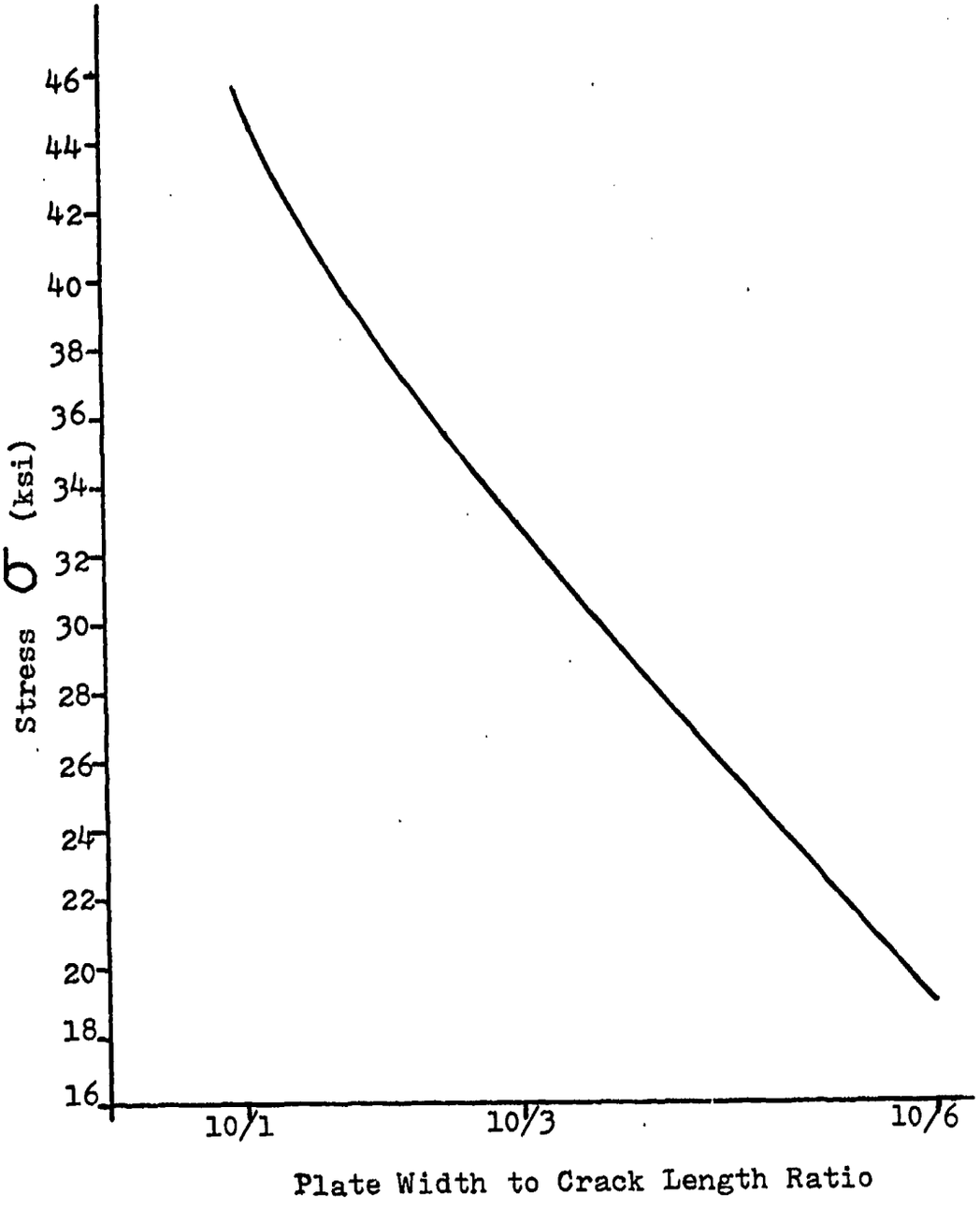

FIGURE 59. Stress Required to Increase a Crack Plotted Against Plate Width to Crack Length Ratio

TABLE VI

Length of Straight Crack Approximation of the Cracks from the 7-HR Series Low Velocity Shots

SHOT	VELOCITY (fps)	APPROX. STRAIGHT CRACK LENGTH (inches)
7-HR-10	1347	4.0
7-HR-11	1386	6.0
7-HR-12	1366	3.5
7-HR-14	1384	5.0

low velocity shots. Since each test plate was 20 inches wide, the data of Table V gives a specimen width to crack length ratio of 10/2.5 for 7-HR-14. Referring to Fig. 59, a ratio of 10/2.5 corresponds to a stress of 35.6 ksi that is required to cause the 5-inch crack to increase. The 5-inch crack corresponds to a half crack length of 2.5 inches and station 6 of the computer model shown in Fig. 50. Since σ_x acts perpendicular to the crack, the σ_x stress at station 6 should be compared to the 35.6 ksi obtained above. The σ_x stress of 11.3 ksi predicted at station 6 is a factor of 3.15 smaller than the 35.6 ksi. This correction factor of 3.15 is, however, well within the range of correction factors obtained above by comparing predicted strains to actual strains, and therefore seems quite reasonable as a correction factor to be used in the prediction of the crack length.

Thus, the method of crack length prediction is as follows: the computer codes are used to predict the stresses in the exit wall. A correction factor, obtained as explained above, is applied to the predicted stresses and the corrected stresses are plotted versus distance from projectile penetration point. Assume various crack lengths and refer to Fig. 59 to find the stress required to increase crack length. The stresses required to increase the crack length are plotted on the same graph as the corrected predicted stresses. The predicted crack length is the crack length at which the predicted stress first falls below the stress required for crack extension. For example, when the correction factor of 3.15 is applied to the σ_x(dry) predictions listed in Table IV, the corrected stresses are those plotted in Fig. 60. Also plotted in Fig. 60 are the stresses required to increase the crack obtained from Fig. 59 for the 20-inch plate. Comparing the two stress plots reveals that the crack length will grow to 5 inches, but no more than that because the stress required to extend the crack beyond 5 inches is greater than the predicted stress. The fact that the predicted crack length is equal to the actual crack length is of course, a consequence of the 3.15 correction factor.

Shots 10, 11, 12, and 14 were all similar enough to use the same computer stress predictions for all four shots. The proposed method of crack length prediction estimated the crack length to be approximately 5 inches long for each shot

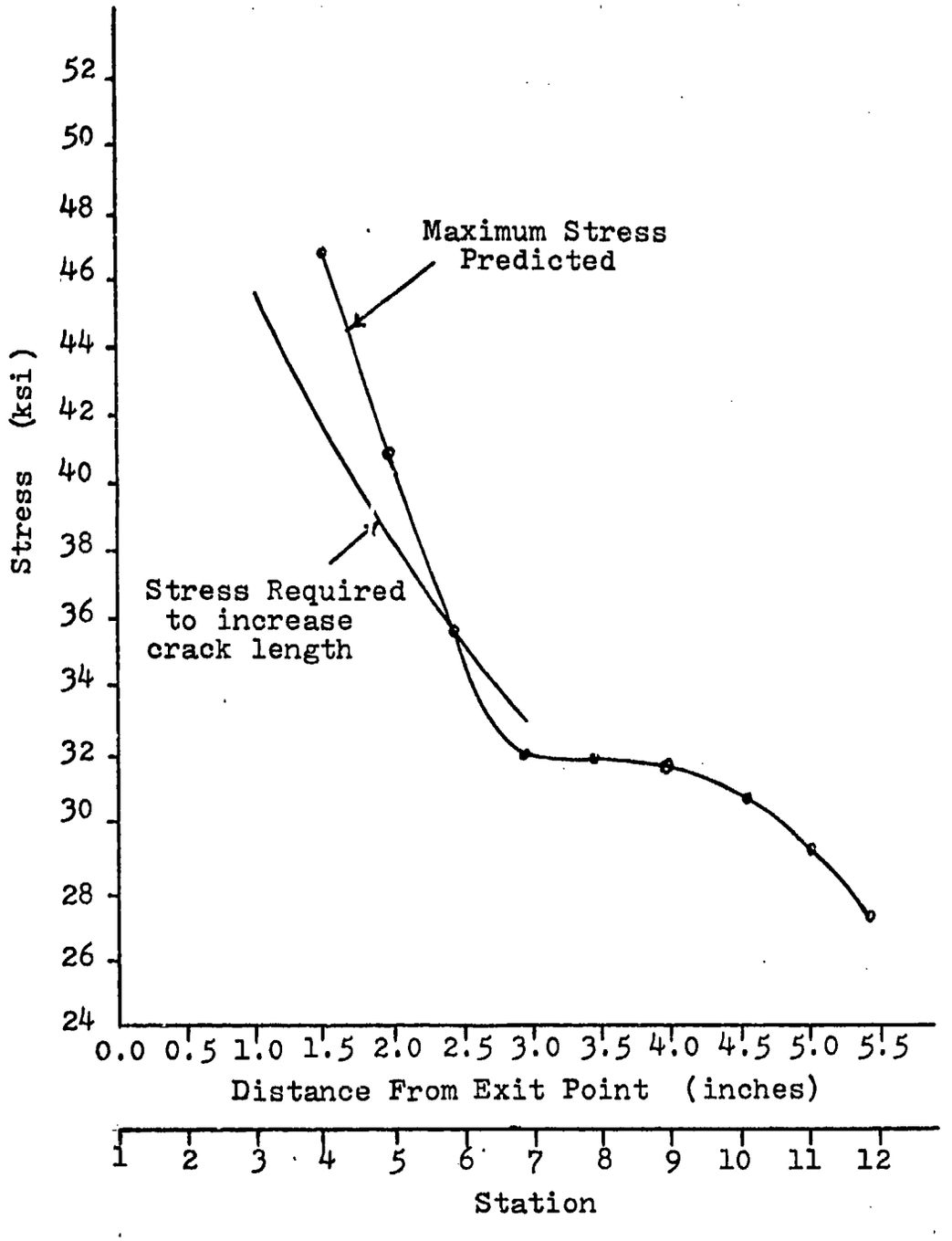

FIGURE 60. Stress Required to Increase Crack Length and Maximum Stress Predicted Plotted Against Distance from Exit Point.

as shown in Fig. 60. Examination of Table VI shows that 7-HR-11 would have exceeded the prediction by 1 inch. However, the other three shots had cracks that were less than the predicted crack length.

C. EXAMINATION OF HIGH SPEED MOTION PICTURES

High speed motion pictures of the exit wall response were available for study for each of the NWC 7-HR series tests. The film speed was 8000 frames per second. From a close examination of the films it was possible to get an estimate of the lapsed time from initial penetration to the time when the cracks reached their maximum length. This data is presented in Table VII. All of the tests are not listed in Table VII because in some cases water spewing from the ruptured tank wall made it impossible to see the cracks. From Table VII it can be seen that the time it took for the cracks to grow to maximum length was between 0.5 and 2.0 msec. The longer cracks taking the longer time to grow. As listed in Table VII, 7-HR-14 had a fracture time of 0.625 msec. Examination of Table VI shows that 7-HR-14 has a crack approximately 5 inches long, or a half-crack length of 2.5 inches, which corresponds to station 6 in Fig. 51. SATANS predicted an elapsed time of 0.95 msec. for the maximum stress to reach station 6 after the projectile penetrated the plate. The 0.625 msec. observed on the films for 7-HR-14 compares quite well with the 0.95 msec. predicted by SATANS.

TABLE VII

Estimated Lapse Time of Crack Process From High Speed Motion Pictures

Shot	Velocity	Estimate Lapse Time of Crack Process (msec)
7-HR-2	2217	1.625
7-HR-3	2254	2.0
7-HR-6	2763	1.375
7-HR-7	2673	2.0
7-HR-8	2643	2.0
7-HR-10	1347	0.5
7-HR-12	1366	0.5
7-HR-14	1384	0.625

VI. CONCLUSIONS AND RECOMMENDATIONS

A. FRACTURE SURFACE EXAMINATIONS

The fractographic examinations of the damaged NWC 7-HR series test plates provided some information about the fracture process that took place as the cracks grew. However, it was not possible to come to any conclusions concerning the process or processes that took place at the point of projectile penetration. The projectile penetration point needs further study in order to determine whether the plate fractures prior to the projectile penetration.

The macroscopic and microscopic examinations of the fracture surfaces resulted in the conclusion that the fractures in the 7-HR series tests were generally ductile shear fractures, and were similar in many respects to the fractures that thin sheets in static tension tests exhibit. This similarity to tensile test specimens may be noteworthy since the time for the fracture process is generally under 2 msec. This may indicate that the strain rate effects of the fracture process are not important. Further investigation into the strain rate effects are necessary to validate the use of static tensile test data in the fracture criterion.

The fracture process itself deserves further investigation with different test parameters to confirm the characterization of the fractures as being ductile shear fractures and to more

firmly establish the similarity to static tensile test fractures. Eventually, temperature effects will also need to be considered because of the diverse temperature environment in which aircraft must operate.

B. CRACK LENGTH PREDICTION METHOD

This study proposes a macroscopic method that would allow the prediction of cracks caused by hydraulic ram phenonoma acting on the exit wall of a fluid containing tank. The method compares computer predicted stresses, which have been modified by an empirical correction factor, with tensile test data on the stress required to cause a crack in a plate to increase. A detailed statement of the method is contained in Section V.B. The discussion in Section V.B. points out that the method provides accurate crack length predictions for the NWC 7-HR series low velocity shots. This close comparison to the actual test results is very encouraging in view of the many simplifying assumptions that have been made in developing the method. Although the method predicts a crack of a certain number of inches, it should be used at the present time to obtain an idea of the relative size of the expected crack length as small, medium, or large: small being a crack length of about 25% of the plate width; medium being a crack length of between 25% to 50% of the plate width; and large being crack lengths larger than 50% of the plate width.

There are several areas that need further investigation in order to improve the method. First and probably most important the computer codes must be improved so that the predictions agree with the actual measurements and the correction factor can be discarded. Also, the method needs to be applied to the medium and high velocity shots of the NWC 7-HR series tests. Additional tests at each velocity level with different plate thicknesses are also required to validate the method. After the method has been validated for the 2024-T3 aluminum considered in this study, other materials such as 7075-T6 aluminum must be examined.

C. SIMPLIFIED DAMAGE PREDICTION

In this study of the cracking of the exit wall a particular feature has been noted. The damage to the exit walls caused by projectiles with initial velocity greater than approximately 2200 fps was considerably greater than the damage caused by projectiles at less than 2200 fps. This feature occurred on both the 0.125 inch thick 7-HR plates (Table III) and on the 0.063 inch thick 6-HR plates (Figs. 2-5) tested by NWC. This appears to be more than coincidence and suggests that there is a consistent "ballistic velocity" that divides the damage into small and large categories. This feature should be investigated further since, if true, it would considerably simplify the analysis required to predict damage.

LIST OF REFERENCES

1. McKenzie, J. R., "Survey and Bibliography of Aircraft Survivability - Vulnerability Research with Emphasis on Hydraulic Ram," Master Thesis, Naval Postgraduate School (NPS), December 1973.

2. Naval Weapons Center, NWC TP 5227, "Fluid Dynamic Analysis of Hydraulic Ram," by E. A. Lundstrom, July 1971.

3. McDonnell Douglas Corporation, Report 6964, F-76-76-555, "Hydraulic Ram: A Fuel Tank Vulnerability Study," by R. Yurkovich, September 1969.

4. Boeing Company, FAD S-66, "Hydraulic Ram," by R. J. Bristow and J. F. Lundeberg, February 1969.

5. Joint Technical Coordinating Group/Aircraft Survivability, JTCG/AS 74-T-018, "Fluid Dynamic Analysis of Hydraulic Ram IV (Users Manual for Pressure Wave Generation Model)," by E. A. Lundstrom and W. K. Fung, December 1974.

6. Joint Technical Coordinating Group/Aircraft Survivability, JTCG/AS 73-T-291, "Fluid Dynamic Analysis of Hydraulic Ram II (Results of Experiments)," by E. A. Lundstrom and E. W. Stull.

7. Joint Technical Coordinating Group/Aircraft Survivability, JTCG/AS 74-T-20 (I), "Analysis of Hydraulic Ram-Structural Response I (Results of Experiment)," by W. K. Fung, December 1974.

8. Bates, K. S. Jr., "Aircraft Fuel Tank Entry Wall-Projectile Interaction Studies," Master Thesis, NPS, June 1973.

9. Holm, D. P., "Hydraulic Ram Shock Wave and Cavitation Effects on Aircraft Fuel Cell Survivability," Master Thesis, NPS, Sept. 1973.

10. Soper, W. R., "Hydraulic Ram Studies," Master Thesis, NPS, December 1973.

11. Fuhs, A. E., Ball, R. E., Power, H. L., "FY 73 Hydraulic Ram Studies," NPS-57Fu74021, Feb. 1974.

12. Mueller, L. S., "Experiments in Hydraulic Ram," Master Thesis, NPS, March 1974.

13. Kappel, L. C., "Hydraulic Ram Shock Phase Effects on Fuel Cell Survivability," Master Thesis, NPS, March 1974.

14. Power, H. L., "FY 74 Experimental Hydraulic Ram Studies," NPS-57Ph74081, Aug. 1974.

15. Holm, C. M., "Hydraulic Ram Pressure Measurements," Master Thesis, NPS, Dec. 1974.

16. Page, B., "Entry Wall Strain Measurements During Hydraulic Ram," Master Thesis, NPS, March 1975.

17. Patterson, J. W., "Fuel Cell Pressure Loading During Hydraulic Ram," Master Thesis, NPS, June 1975.

18. Power, H. L., "FY 75 Experimental Hydraulic Ram Studies," NPS-57Ph75061, June 1975.

19. Ball, R. E., Power, H. L., and Fuhs, A. E., "Fuel Tank Wall Response to Hydraulic Ram During The Shock Phase," Journal of Aircraft, Vol. 10, No. 9, pp. 571-572, Sept. 1973.

20. Ball, R. E., "Prediction of the Response of the Exit Wall of the NWC 50 Cubic Feet Tank to Hydraulic Ram," NPS-57Bp 74031, March 1974.

21. Ball, R. E., "A Discussion of Dynamic Crack Propagation in Bent Plates," NPS-57Bp74041, April 1974.

22. Bitzburger, J. C., "Two-Dimensional Analysis of Fluid-Structural Interation by Method of Finite Differences - Hydraulic Ram, The Fuel Tank Problem," Master Thesis, NPS, June 1974.

23. Ball, R. E., "Aircraft Fuel Tank Vulnerability to Hydraulic Ram: Modification of the Northrup Finite Element Computer Code BR-1 to Include Fluid-Structure Interaction -- Theory and User's Manual for BR-1HR," NPS-57Bp74071, July 1974. (AFFDL funding)

24. Ball, R. E., "A Computer Program for the Geometrically Nonlinear Static and Dynamic Analysis of Arbitrarily Loaded Shells of Revolution, Theory and User's Manual," NASA CR-1987, April 1972..

25. Ball, R. E., "Structural Response of Fluid Containing Tanks to Penetrating Projectiles (Hydraulic Ram) - A Comparison of Experimental and Analytical Results," NPS-57Bp75101, December 1975.

26. Drucker, D. C., "A Continuum Approach to the Fracture of Metals," Metallurgical Society Conferences, Vol. 20, Fracture of Solids, Ed. D. C. Drucker and J. J. Gilman, Interscience Publishers, 1963.

27. Yokobori, T., An Interdisciplinary Approach to Fracture and Strength of Solids, p. 122-185, Walters-Noordhoff Scientific Publications Ltd., 1968.

28. Tetelman, A. S. and McEvily, A. J. Jr., Fracture of Structural Materials, p. 38-82, John Wiley and Sons, Inc., 1967.

29. Metals Handbook, 8th ed. V. 9, American Society for Metals, 1964.

30. Ryder, D. A. and Smale, A. C., "A Metallographic Study of Tensile Fractures in Aluminum-Copper and Aluminum-Copper-Zinc-Magnesium Alloys," Metallurgical Society Conferences, Vol. 20, Fracture of Solids, Ed. D. C. Drucker and J. J. Gilman, Interscience Publishers, 1963.

31. Orwin, G. R., Fracturing of Metals, p. 147, ASM, Metals Park, Ohio, 1948.

32. Orowan, E., Reports on Progress in Physics, V. 12, p. 185, 1949.

33. Eftis, J., Jones, D. L., and Liebowitz, H., "Basic Concepts in Fracture Mechanics," AGARDograph No. 176 on Fracture Mechanics of Aircraft Structures, Ed. H. Liebowitz, Technical Editing and Reproduction Ltd., 1974.

34. Damage Tolerant Design Handbook, Metals and Ceramics Information Center (MCIC), Columbus, 1972.

INITIAL DISTRIBUTION LIST

		No. Copies
1.	Defense Documentation Center Cameron Station Alexandria, Virginia 22314	2
2.	Library, Code 0212 Naval Postgraduate School Monterey, California 93940	2
3.	Department Chairman, Code 57 Department of Aeronautics Naval Postgraduate School Monterey, California 93940	1
4.	Dr. R. E. Ball, Code 57Bp Department of Aeronautics Naval Postgraduate School Monterey, California 93940	4
5.	Lt. S. L. Fahrenkrog 115 Malloway Lane Monterey, California 93940	1